VILNIUS UNIVERSITY

Milda
ALKSNĖ

Substrate-dependent fate of stem cells: insights into artificial bone fabrication

SUMMARY OF DOCTORAL DISSERTATION

Natural Sciences,
Biochemistry N 004

VILNIUS 2020

This dissertation was written between 2014 and 2019 in Vilnius University Life Sciences Center.

Academic supervisor:
Dr. Virginija Bukelskienė (Vilnius University, Natural Science, Biochemistry – N 004).

Defense board:

Chairman:
prof. dr. Vytautė Pečiulienė (Vilnius University, Medicine and Health Sciences, Odontology – M 002).

Members:
prof. dr. Genė Biziulevičienė (Centre for Innovative Medicine, Natural Sciences, Biology – N 001);
dr. Veronika Viktorija Borutinskaitė (Vilnius University, Natural Sciences, Biochemistry – N 004);
prof. dr. Vytautė Starkuvienė-Erfle (Heidelberg University, Natural Sciences, Biochemistry – N 004);
prof. dr. Arvydas Ūsas (Lithuanian University of Health Sciences, Natural Sciences, Biochemistry – N 004).

The dissertation shall be defended at a public/closed meeting of the Dissertation Defence Panel at 13 h/ on 31 March 2020 in Vilnius University Life Sciences Centre in auditorium R-101.

Address: Saulėtekio av. 7, LT- 10257 Vilnius, Lithuania.
Tel.: +370 5 223 4420. Email: info@gmc.vu.lt

The text of this dissertation can be accessed at the library of Vilnius University, as well as on the website of Vilnius University: www.vu.lt/lt/naujienos/ivykiu-kalendorius

VILNIAUS UNIVERSITETAS

Milda
ALKSNĖ

Nuo substrato priklausantis kamieninių ląstelių likimas: įžvalgos dirbtinio kaulinio audinio kūrimui

DAKTARO DISERTACIJOS SANTRAUKA

Gamtos mokslai,
biochemija N 004

VILNIUS 2020

Disertacija rengta 2014–2019 metais Vilniaus universiteto Gyvybės mokslų centre.

Mokslinė vadovė:
dr. Virginija Bukelskienė (Vilniaus universitetas, gamtos mokslai – biochemija – N 004).

Gynimo taryba:

Pirmininkė:
prof. dr. Vytautė Pečiulienė (Vilniaus universitetas, medicinos ir sveikatos mokslai, odontologija – M 002).

Nariai:
prof. dr. Genė Biziulevičienė (Inovatyvios medicinos centras, gamtos mokslai, biologija – N 001);
dr. Veronika Viktorija Borutinskaitė (Vilniaus universitetas, gamtos mokslai, biochemija – N 004).
prof. dr. Vytautė Starkuvienė-Erfle (Heidelbergo universitetas, gamtos mokslai, biochemija – N 004).
prof. dr. Arvydas Ūsas (Lietuvos sveikatos mokslų universitetas, gamtos mokslai, biochemija – N 004).

Disertacija ginama viešame Gynimo tarybos posėdyje 2020 m. kovo mėn. 31 d. 13 val. Vilniaus universiteto Gyvybės mokslų centre, R-101 auditorijoje.

Adresas: Saulėtekio al. 7, LT-10257, Vilnius, Lietuva. Tel.: +370 5 223 4420. Email: info@gmc.vu.lt

Disertaciją galima peržiūrėti Vilniaus universiteto bibliotekoje ir VU interneto svetainėje adresu: *https://www.vu.lt/naujienos/ivykiu-kalendorius*

THE LIST OF ABBREVIATIONS

ALP – Alkaline Phosphatase
ARS – Alizarin red S
BG – Bioglass
BMSC – Bone marrow-derived mesenchymal stem cells
BSA – Bovine serum albumins
CCL5 – Chemokine (C-C motif) ligand 5
CINC – Cytokine-induced neutrophil chemoattractant
CX3CL1 – Chemokine (C-X-C motif) ligand 1
CXCL10 – C-X-C motif chemokine 10
DMEM – Dulbecco's modified Eagle medium
DMSO – Dimethyl sulfoxide
DPSC – Dental pulp-derived stem cells
EDTA – Ethylenediaminetetraacetic acid
PBS – Phosphate-buffered saline
FFF – Fused Filament Fabrication
FBS – Fetal Bovine Serum
GAPDH – Glyceraldehyde-3-phosphate dehydrogenase
HA – Hydroxyapatite
YAP – Yes-associated protein
IL-1ra – Interleukin-1ra
IL-6 – Interleukin-6
IMDM – Iscove's Modified Dulbecco's Medium
GM – Growth medium
MSC – Mesenchymal stem cells
NDS – Sodium dodecyl sulfate
OCN – Osteocalcin
OPN – Osteopontin
PLA – Polylactic acid
Runx2 – Runt-related transcription factor 2
SEM – Scanning electron microscope
sICAM-1 –Soluble intercellular adhesion molecule-1
SSC – Saline sodium citrate
TIMP-1 – TIMP metallopeptidase inhibitor 1
ECM – Extracellular matrix
VEGF – Vascular endothelial growth factor

1. INTRODUCTION

To ensure basic physiological processes of the organism, cells in tissues should interact with each other and with the extracellular environment (i.e. extracellular matrix - ECM). Moreover, to maintain homeostasis in the organism, they should respond to the behaviour of neighbouring cells and feel the changes of the ECM. Stem cells, harbouring in the tissues, play a special role in the organism's regeneration processes. By sensing alterations in the ECM, stem cells are able to differentiate in the required direction to repair damaged tissue.

To understand the mechanisms of all these processes, various *in vitro* models that mimic many biological phenomena, such as cell-cell or cell-ECM interactions, are being developed. Knowledge of such biological contacts and their impact on cell fate is important both theoretically and practically. Thus, findings about cell-ECM interplay can be applied for artificial tissue construction in practice.

Loss of organs/tissues or disruption of their functions, which can largely depend on "inappropriate" cell interactions, is one of the biggest problems in medicine. Currently, such diseases are treated by organ/tissue transplantation. Although this procedure has helped hundreds of thousands of patients, doctors are still unable to guarantee successful tissue or organ integration after the transplantation. Therefore, tissue or organ transplantation is usually carried out only in cases when there is no other way to save human life. Moreover, the most common problem of transplantation is the lack of donor tissues or organs. According to the National Transplant Bureau under the Ministry of Health, 475 patients, 19 of whom are children, were waiting for a transplant in Lithuania on December 16, 2019. Meanwhile, there have been only 51 effective donors this year.

Although bone tissue is capable to regenerate naturally, its need in transplant surgery is no exception. Millions of people annually worldwide are affected by a loss of bone tissue because of the bone

defects and deficiencies that are formed due to trauma, inflammation, tumours or genetic diseases, when bone is no longer capable of self-repair. To treat these bone defects, bone grafts are considered the "gold standard". There are three major categories of materials which are commonly used in bone grafting surgical procedures: autografts, allografts and xenografts. Yet, the use of auto-, allo- and xeno-grafts has some disadvantages. Autografts suffer from limited resource and donor-site morbidity due to potential infection and haematoma; moreover, harvesting requires an additional surgical procedure. While problems associated with allografts and xenografts can be pathogen transmission to the patient and immunological rejection by the recipient's body. Therefore, using the latest tissue engineering achievements, scientists are seeking to create patient-specific, biocompatible, osteoconductive, and osteo- and angio-inductive artificial stem cells and scaffold derivatives (constructs) which ensure effective diseased bone tissue regeneration. Moreover, it is desired that constructs manufacture process would be inexpensive and high in production speed.

Bone tissue constructs that meet these criteria can be manufactured by combining polymeric (such as polylactic acid (PLA), etc.) and bioceramic (hydroxyapatite (HA), bioglass (BG), etc.) materials with one of the most promising technologies – fused filament fabrication (FFF) 3D printing. 3D printing technology is becoming more and more inexpensive and adaptable in tissue engineering applications, thus selecting proper materials and awareness of their biological properties, as well as impact on cell fate, is becoming a significantly important topic.

To produce osteoconductive, osteo- and angio-inductive artificial bone, it is not enough to select right materials combinations and optimal scaffold production method. To facilitate artificial bone construct integration into patient's organism, the scaffold should be also enriched with active biological molecules and/or pre-seeded with autologous patient‘s stem cells.

One of the most promising method for scaffold surface decoration is autologous cell-derived extracellular matrix (ECM) coating. Such ECM network enriches scaffold with a variety of signalling and structural protein molecules, making its surface more attractive for cell attachment, migration, or even differentiation. Scaffold coating with cell-derived ECM is a rapidly growing field of research, but until now the role of such ECM in bone tissue regeneration has been investigated using only a few types of cell cultures and scaffolds.

For personalized artificial bone construction and cell-scaffold interaction studies the most widely used cell type is mesenchymal stem cells (MSC). Dental pulp stem cells (DPSC) are an adult mesenchymal stem cell source that possesses high proliferative, self-renewal, and multipotency capabilities. Importantly, DPSCs tend to spontaneously differentiate into osteogenic lineage. All these properties make DPSCs a perfect autologous MSC choice for this kind of studies.

In this work we analysed various FFF 3D-printed PLA scaffold modifications' impact on cell fate. Rat DPSCs were selected as a model, which helped to understand the cellular responses to different substrate modifications. PLA scaffolds were modified by altering their topography, chemical composition, and surface coating with proteins in order to determine the impact of each substrate modification on cell functions and properties, focusing on cell osteogenesis processes.

1.1 Aim of the study

To determine the influence of different substrate modifications on the fate of stem cells for construction of functional artificial bone tissue.

1.2 Study objectives

1. To investigate the role of surface macrotopography (> 100 μm) in the fate of dental pulp stem cells (DPSC).
2. To evaluate the impact of substrate chemical composition on DPSC vital processes.
3. To analyze the role of chemical composition of the material in cell osteogenesis.
4. To determine the effect of substrate bio-decoration on DPSC cell motility, attachment and proliferation.
5. To evaluate the impact of surface decoration on cell osteogenic differentiation.
6. To model and evaluate the signal sent by the construct to the recipient tissues under *in vitro* conditions.

1.3 Novelty of the study

Until now it was known that only nano- and microsurface topographies can regulate cell fate. In this work, it was demonstrated that FFF 3D printed macrosurface topographies (> 100 μm) are sufficient enough to initiate spontaneous stem cells osteogenic differentiation. This proves that FFF 3D printing can be successfully applied for cheaper, faster and personalised production of scaffolds for artificial bone tissue.

Furthermore, for the first time physical and osteoinductive properties of FFF 3D printed PLA+HA and PLA+BG scaffolds were compared. It was determined that PLA+BG composite is more suitable for artificial bone tissue construction. These results will contribute to optimizing artificial bone tissue construct production.

Promising scaffold decoration technology – surface coating with cell-derived ECM– was also investigated in this work. Here, for the the first time this technology was applied using primary DPSCs and

FFF 3D printed PLA scaffold. It was observed that DPSC-derived ECM significantly improves osteoinductivity of the scaffold *in vitro*.

Moreover, using *in vitro* methods, evaluating the potential of different constructs' (cell-scaffold) signals to the organism was attempted. This was the first time then this kind of study was performed to compare constructs made from primary DPSCs and PLA+HA, PLA+BG, PLA+ECM scaffolds. It was shown that DPSC-PLA+BG and DPSC-PLA+ECM constructs should ensure the best bone regeneration. Therefore, we believe that by combining DPSCs, macroporous PLA+BG scaffold and DPSC-derived ECM, successful bone tissue regeneration can be expected *in vivo*.

This scientific work significantly contributes to bone regenerative medicine progress which would lead to a breakthrough in new generation medicine.

2. MATERIALS AND METHODS

2.1 Materials

Sigma-Aldrich Co.: Ethylenediaminetetraacetic acid (EDTA); dimethylsulfoxide (DMSO); L- ascorbic acid 2-phosphate; trisodium citrate dihydrate; sodium dodecyl sulfate (SDS); 50 wt. % glutaraldehyde; TWEEN 20; 1,3 % picric acid; 99, % isopropanol; polybrene; Crystal violet; alizarin red S (ARS); oil red O; Direct Red 80.

Thermo Scientific: 50 mM EDTA; DNaze I (#EN0521); RNaze A, 10 mg/ml (#EN0531); Phosphatase Substrate Kit (#37620); Maxima SYBR Green/ROX qPCR Master Mix (2X) (#K0221); Lipofectamine 3000 Reagent.

Invitrogen: UltraPure Glycine; PureLink RNA Mini Kit (12183018A); goat ant-mouse secondary IgG (H+L) antibody, Alexa Fluor 488 conjugated.

Applied Biosystems: High capacity cDNA Reverse Transcription Kit (00506262).

AppliChem GmbH: 70 % perchloric acid; Triton X-100; bovine serum albumins (BSA); 96% acetic acid; 37 % hydrochloric acid (HCl).
Life Technologies: TRIzol; 4',6-Diamidino-2-phenylindole dihydrochloride (DAPI).
Gibco: Phosphate-buffered saline (PBS) tablets; Iscove's Modified Dulbecco's Medium (IMDM); Dulbecco's Modified Eagle Medium (DMEM); fetal bovine serum (FBS); penicillin-streptomycin (10,000 units/ml and 10,000 μg/ml, respectively) solution.
Carl Roth, GmbH: 4 % paraformaldehyde solution.
Valentis: 10 % ammonia (NH4OH).
R&D Systems: Proteome Profiler Rat Cytokine Array Kit, Panel A (ARY008).
Addgene: lentiviral vectors - pLJM1-mCherry, pCMV-dR8.9, pCMV-VSV-G.
Nanodiagnostika: qPCR primers.
Decon Laboratories Limited: Decon-90.
Vilniaus degtinė: 96 % ethanol (EtOH).
Merck Millipore: rhodamine phalloidin; primary anti-Vinculin mouse antibody.
ATCC: HEK293T cell line.
Ultimaker Original: PLA filament.
STP chem solutions co.: Ltd. PLA beads.
Riga Technical University: HA powder.
XL Sci-Tech, Inc: BG 45S5 beads.

2.1.1 Solutions

DPSC and PKEL growth medium: IMDM, 10 % FBS, 100 units/ml penicillin and 100 μg/ml streptomycin.
HEK293T growth medium: DMEM, 10 % FBS, 100 units/ml penicillin and 100 μg/ml streptomycin.
PKEL-R selection medium: DMEM, 10 % FBS, 100 units/ml penicillin and 100 μg/ml streptomycin and 5 μg/ml puromycin.
EDTA/trypsin solution: 0.02 M EDTA and 0.025 % trypsin solution; prepared in a ratio 4:1.

Crystal violet dye: 0.1 % crystal violet solution, prepared in 20 % EtOH.
Elution buffer: 0.1 % acetic acid, diluted in 50 % EtOH.
ARS dye solution: 2 % ARS, diluted in deionized water pH = 4.1–4.3. Required pH was adjusted with NH_4OH or H_2SO_4.
Ascorbic acid solution: 5 mg/ml L- ascorbic acid 2-phosphate, diluted in PBS.
20x sodium citrate buffer (SSC): 3M NaCl and 0.3 M trisodium citrate solution; prepared in deionized water, pH = 7.0. Required pH was adjusted with 10 M NaOH.
Lysis solution: 0.02 % SDS solution, prepared in 1x SSC solution
Decellularization solution: 0.5 % Triton X-100 and 20 mM NH_4OH; prepared in PBS.
Blocking solution: 3 % BSA and 10 % FBS solution; prepared in PBS.
Sirius Red dye: 1 mg/ml Direct Red 80, diluted in 1.3 % picric acid
Nuclease solution: 0.5 % Triton X-100 and 20 mM NH4OH, prepared in PBS

2.2 Methods

2.2.1 Cell culture isolation and cultivation

Rat DPSCs and PKELs were used for this study. The use of rat DPSCs and PKELs as well as their extraction procedure was approved by license of Animal research ethics committee (Lithuania) No. G2-40, 2016-03-18. Cell isolation and characterisation protocols are described in (Alksne et al., 2019). Isolated DPSCs and PKELs were maintained in growth medium at 37 °C in a humidified atmosphere containing 5 % CO_2. The cells used in the experiments were up to 20 passages.

2.2.2 Genetic modification of cells

2.2.2.1 Lentivirus production

Lentivirus production was performed using the HEK293T (human embryonic kidney cell line, that expresses a mutant version of the SV40 large T antigen) cell line. The packaging (pCMV-dR8.91), envelope (pCMV-VSV-G) and target (pLJM1-mCherry) protein coding lentivirus vectors were used for lentivirus production.

Briefly, HEK293T lentivirus packaging cells ($7 \cdot 10^4$ cell/cm^2) were seeded into cell culture plate and cultured overnight at 37 °C in a humidified 5 % CO2 atmosphere. After predetermined time, when cells reached 70–80% confluence, HEK293T transfection was performed using Lipofectamine 3000 reagent. The transfection procedure was performed according to the manufacturer's protocol. A mixture of lentiviral vectors was prepared at a mass ratio of 2:1.2:0.8 (pLJM1-mCherry:pCMV-dR8.91:pCMV-VSV-G). After 18 h, the media was replaced with a growth media modified to contain 20% FBS, and the virus was harvested at 24 h after the media switch. Harvested media with virus was transferred to a glass tube with polybrene (8 μg / ml). The resulting mixture was filtered through a 0.22 μm filter. The filtered suspension was stored at -80 ° C until use.

2.2.2.2 Lentiviral transduction

Red fluorescent PKELs (PKEL-R) were generated by transducing produced lentivirus into PKELs.

PKELs were plated at a density of $1 \cdot 10^4$ cell/cm^2. The next day, prepared lentivirus-polybrene mixture was transferred to PKELs at volume ratio 1:2 (lentivirus-polybrene mixture:GM). After 24 h, the

media was replaced with normal GM and cells were cultured for another 24 h. After predetermined time, the GM was replaced with selection media (containing puromycin), where cells were grown for 3-5 days. During these days, successfully transduced cells formed red (PKEL-R) fluorescent cell culture.

2.2.3 Scaffold production and analysis of their characteristics

2.2.3.1 3D printing of scaffolds with differently macro-structured surface

For distinctly macro-structured scaffold preparation a clear (pure) PLA material was used. Scaffolds were printed using FFF 3D printer "Ultimaker" Original (Ultimaker B.V.).

Briefly, the nozzle diameter was 400 μm. The operating temperature was set to 180–190°C, and the pinpoint scanning velocity was set to 30 mm/s. The printing bed was of room temperature, and the cooling fan rate was set to 65 of its capacity (default value). Scaffold structures were created using the AutoCAD 2017 software package and the resulting models were saved in STL format. STL format models were converted to g-code by the 3D printer software.

Two different scaffolds were manufactured: with porous and wavy topography. The obtained line width and height were: 500 μm and 188 μm; 188 μm and 250 μm, respectively. The dimensions of 3D printed scaffolds were 3 cm x 3 cm x 1.6 mm. For *in vitro* studies, scaffolds were cut into 1 cm x 1 cm x 1.6 mm pieces.

Before use, scaffolds were immersed in Decon-90 for 24 h, washed 30x with distilled water and immersed in 96 % EtOH for another 24 h. After predetermined time, scaffolds were maintained under UV light for 1 h.

2.2.3.2 Composite filament preparation

Raw materials used for composite filament preparation were PLA (racemic polymer composed of D and L isoforms) beads – particle size 100 – 800 μm, molecular weight 42 700 (g/mol); HA powder - particle size 50 μm; and BG 45S5 - particle size 38-75 μm.

Composite materials were prepared by thoroughly mixing the PLA and HA or PLA and BG powders at mass ratio of 9:1; in the case of pure PLA filament, only PLA pellets were used. Before extrusion, the mixture was stored in a sealed bag with silica gel pellets to absorb all the moisture from the material, as otherwise, the extrusion process was hard to control due to bubble formation in the filament. A desktop extruder (Filabot Original, Filabot HQ) equipped with a 1.75 mm nozzle was used to fabricate the filament. The extruder was pre-heated to 145 °C. A self-made spooler with adjustable spooling speed was used to wind the filament onto the reel. During the extrusion process, the temperature of the extruder was manually adjusted in the range of 140 – 145°C when needed. The diameter of the prepared composite filament varied from 1.28 to 1.6 mm.

2.2.3.3 Composite scaffold production

Composite scaffolds were fabricated using an FDM 3D printer 2 (Pharaoh XD 20, Mass Portal). The printing head was computer-controlled in three axes of delta mode (x, y, z with a xyz speed of 35 mm/s). The nozzle diameter was 400 μm. Scaffolds were designed with a pore size of 450 μm and a total porosity of 48 %. The scaffold geometry was a 3D macro-structured woodpile with threads rotated at an angle of 60° in respect to the ones of the previous layer. Each

scaffold layer consists of two 400 μm width and 200 μm height threads moulded together, which formed a 400 μm height layer. All scaffolds had eight layers (Fig. 1A). The dimensions of 3D printed scaffolds were 3 cm x 3 cm x 1.6 mm. For *in vitro* studies, scaffolds were cut into 1 cm x 1 cm x 1.6 mm pieces.

Before use, scaffolds were immersed in Decon-90 for 24 h, washed 30x with distilled water and immersed in 96 % EtOH for another 24 h. After predetermined time, scaffolds were maintained under UV light for 1 h.

2.2.3.4 Decellularized PLA scaffolds production

To produce PLA scaffolds coated with cell-derived ECM, DPSCs suspension ($3 \cdot 10^4$ cell/cm^2) were seeded on pure PLA scaffolds. Cells-scaffold constructs were cultivated for 7 days in GM containing 100 μg/ml ascorbic acid solution, half of media was changed every second/third day. After 7 days, scaffolds were washed 2x with PBS and transferred to -20 °C freezer for 30 min. After that, decellularization solution was added onto the samples, incubated for 1 h with gentle shaking (25 rpm, with Biometra WT 17) at 37 °C. After that, decellularization solution was aspirated, specimens were rinsed 2x with PBS and nuclease solution was added, incubated for 1 h with gentle shaking (25 rpm) at 37 °C. After predetermined time, nuclease solution was aspirated and samples were washed 2x with PBS. After washing step, the 0.1 % glutaraldehyde solution (prepared in PBS) was added, incubated 4-6 h at 4 °C. After incubation, specimens were rinsed with PBS and immersed in 0.1 M glycine solution (prepared in PBS), incubated over night at 4 °C. The next day, samples were washed again 2x with PBS and stored in PBS at 4 ° C until use.

2.2.3.5 SEM imaging

A scanning electron microscope (Hitachi TM-1000) was used to analyse the surface and morphology of the scaffolds. The sides of the prepared scaffolds were prepared by cutting specimens with laser light filament fabrication technology, 10 mm from the sides. Scaffolds were scanned edgewise (15 images in total for each group). Thread height, width and distance between threads were measured using ImageJ (1.8.0_112).

2.2.4 Analysis of cell-scaffold interaction

2.2.4.1 Evaluation of cell morphology and adhesion

In order to determine DPSCs behaviour on tested scaffolds the qualitative and quantitative evaluation of cell morphology and adhesion was performed by seeding DPSCs ($5 \cdot 10^4$ cell/cm^2) on scaffolds and visualizing the F-actin filaments presented within the cells. For that purpose, DPSC were grown on PLA scaffolds for 2 and 24 h. After predetermined time points, samples were fixed with 4% paraformaldehyde at room temperature for 15 min with gentle agitation (25 rpm). Then samples were rinsed 3x for 5 min with 0.2% Triton X-100 in PBS and stained with 5 U/mL rhodamine phalloidin and 12.5 μg/mL DAPI working solution in PBS in a dark for 60 min at room temperature. After incubation, samples were rinsed 3x for 5 min with PBS. Specimens were visualized by fluorescence inverted microscope (Olympus IX51).

Differences in cells' morphology and shape were evaluated by measuring cells and their nucleus aspect ratios (relationship between the width and height) using image processing program ImageJ (ImageJ 1.8.0_112).

Quantitative differences in cells' adhesion efficiency were calculated by measuring the DPSCs surface area on different scaffolds at predetermined time points using an image processing program ImageJ (1.8.0_112).

2.2.4.2 Cellular adhesion strength

DPSCs adhesion strength on tested scaffolds was qualitatively and quantitatively evaluated by visualising focal adhesions (FA) within the cells 24 h after seeding ($5x10^4$ cell/cm^2) on different scaffolds. Cultured cells were fixed with 4 % paraformaldehyde solution for 15 min at room temperature with 25 rpm shaking. Then samples were washed 3x with 0.2 % Triton X-100 in PBS for 5 min at room temperature and blocked for 1 h with blocking solution. After blocking procedure, specimens were incubated with primary mouse anti-vinculin antibody (1:50) for 1 h at room temperature with 25 rpm shaking. Then, samples were washed 3x with 0.05 % Tween-20 in PBS for 5 min and incubated with secondary goat anti-mouse antibodies conjugated with Alexa Flour 488 (1:500) and 12.5 µg/mL DAPI solution in PBS for 1 h at room temperature in the dark with 25 rpm agitation. The samples were washed 3x with PBS for 5 min at room temperature and visualised by fluorescence inverted microscope (Olympus IX51). Quantitative differences in cell adhesion strength were determined by counting FA within the cells using image processing program ImageJ (1.8.0_112).

2.2.4.3 Cell migration

For evaluation of cell migration on tested scaffolds, vertical cell migration assay was performed. For this reason, DPSCs or PKELs ($5x10^4$ cell/cm^2) were seeded in tissue culture plate wells. After 24 h,

tested scaffolds were placed on the formed cell monolayer and incubated for 72 h. Then, specimens were transferred to the new plate wells and washed with PBS. The numbers of cells which have migrated on each scaffold were determined by Crystal Violet assay. Briefly, samples were stained with crystal violet dye for 30 min with 25 rpm shaking. Then, the specimens were washed 3x with deionized water and the crystal violet was dissolved in the elution buffer and incubated for 10 min. Dissolved crystal violet absorbance was measured using a microplate spectrophotometer Varioskan Flash (Thermo Scientific) at 590 nm. In order to evaluate scaffolds background, samples were placed on the cell monolayer for 3 h and then processed as described above.

A qualitative assessment of PKEL migration on scaffolds covered with DPSCs was also performed. Transfected red fluorescing cells, PKEL-R, and unmodified DPSC were used in this study.

In parallel, PKEL-R ($5 \cdot 10^3$ cell/cm^2) and DPSC ($1 \cdot 10^4$ cell/cm^2) were seeded into cell culture plate wells and on the tested scaffolds, respectively. 48 h after seeding, scaffolds with DPSCs were transferred to plate wells where the PKEL-Rs was growing. After 3 and 72 h, scaffolds were transferred to the new plate wells and washed 2x with PBS. Obtained samples were visualised by fluorescence inverted microscope (Olympus IX51).

2.2.4.4 Cell proliferation

In proliferation experiments, DPSCs ($3 \cdot 10^4$ cell/cm^2) were grown on tested scaffolds for 24, 48, 72, 96 and 120 h. Three hours after seeding, scaffolds were transferred to new plate wells containing GM, except cells grown on the cell culture plate surface, whose GM was changed. After predetermined time points, GM was removed, wells were rinsed 2x with PBS solution and plates were transferred to −20°C freezer at least for 1 h. After that, cells were lysed with

0.04% SDS solution prepared in the SSC buffer by shaking (300 rpm) for 30 min at 37°C. Obtained lysates were diluted 2x with SSC and mixed (1:1) with 4 μg/mL DAPI solution in 1xSSC; after 1 h of incubation in the dark by shaking (300 rpm), the DAPI-DNA fluorescence was measured ($\lambda_{excitation}$ = 360 nm, $\lambda_{emission}$ = 460 nm) using a microplate reader Varioskan Flash (Thermo Scientific). Cell number was evaluated by comparing fluorescence intensity to calibration curve values which has been prepared earlier (Figure S1). Results were standardized according to cell number determined on the appropriate scaffolds after 24 h of incubation.

2.2.4.5 Evaluation of cytokines presented in secretomes

In order to evaluate cytokines which were secreted by DPSCs cultivated on tested scaffolds the cytokine expression assay were performed. For this reason, DPSCs ($1 \cdot 10^3$ cell/cm^2) were grown on tested scaffolds for 7 days. After that, scaffolds were rinsed 2x with PBS and transferred to new plate wells containing GM without FBS. After 48 h, GM, with DPSCs secreted cytokines, was collected and centrifuged for 4 min. at 1000 g (HERMLE, Labortechnik GmbH). Supernatants were transferred to new tubes and stored at -20 ° C until use.

Analysis of cytokines presented in collected secretomes was performed using Rat Cytokine Array Kit. All the procedures were performed according to the manufacturer's protocol.

2.2.5 Investigation of cell osteogenesis

2.2.5.1 Induction of osteogenic differentiation

For DPSCs spontaneous osteogenic differentiation evaluation, cells (seeded cell number noted in Table 2.1) were grown on different composite scaffolds for 1, 7 and 10 days. Specimens were maintained in basic GM at 37 °C in a humidified atmosphere containing 5 % CO_2; half of GM was changed every second/third day.

Table 2.1. The amount of cells which were seeded on the scaffolds for analysis of osteogenic differentiation at the corresponding time points.

Day	Cell count
1	$1x10^5$ cell/cm^2
7	$3x10^3$ cell/cm^2
10	$3x10^3$ cell/cm^2

2.2.5.2 Alkaline phosphatase activity

Alkaline phosphatase (ALP) activity was detected using Phosphatase Substrate Kit. Cells grown on tested scaffolds were immersed in 1 mg/ml p-Nitrophenyl phosphate (PNPP) solution and after 1 h of incubation 2 M NaOH (Merck Millipore) was added to stop ALP reaction. The reaction product was measured with spectrophotometer Varioskan Flash (Thermo Scientific) at 405 nm.

As a background value, scaffolds without cells were attributed. Obtained data was normalised according to cell numbers which were determined on each type of scaffold after predetermined time points.

2.2.5.3 Collagen amount

The amount of collagen in the ECM was determined using Sirius red assay. At 1, 7 and 10 spontaneous differentiation days' time points, GM was discarded; specimens were washed 2x with PBS. Then, Sirius Red dye was added to each sample and incubated for 1 h at room temperature with 25 rpm shaking. Afterwards, Sirius Red solution was removed; the samples were washed with 0.01 N HCl in PBS and centrifuged at 100 g for 30 s (centrifuge HERMLE Labortechnik GmbH). Sirius Red residues on the scaffolds were dissolved in 0.1 N NaOH in PBS, by incubating for 30 min at room temperature with 25 rpm shaking. The absorbance was measured using a microplate spectrophotometer Varioskan Flash (Thermo Scientific) at 550 nm. As a background value, scaffolds without cells were used.

2.2.5.4 Osteogenesis-related gene expression

qPCR assay was performed to analyse the expression of Runx2, Osteopontin (OPN) and Osteocalcin (OCN) genes in differentiated DPSC. The qPCR assay was performed after induced and spontaneous osteogenic differentiations at predetermined time points. At each time interval, cells-PLA constructs were rinsed with PBS and afterwards lysed with TRIzol Reagent. For successful removal of lysate, PLA scaffolds were centrifuged at 200g for 5 min (HERMLE, Labortechnik GmbH). Total RNA from each time interval was isolated using a PureLink RNA Mini Kit according to product

manual. For each sample, extracted RNA was transcribed into cDNA using a RevertAid First Strand cDNA Synthesis Kit according to manufacturer's instructions. qPCR was performed by using Maxima SYBR Green/ROX qPCR Master Mix (2×). Total volume of reaction was reduced to 10 μL, thus 1 μL of prepared cDNA was used and a final concentration of primers in the reaction was 0.2 μM. Each primer was designed with NCBI/ Primer-BLAST (Table 2.2). qPCR reactions were run on the Rotor Gene Q (Qiagen). After initial denaturation for 3 min at 95°C, qPCR amplifications were carried out for 30 s at 95°C, 30 s at 57°C and 30 s at 72°C for 40 cycles. Reaction was ended by samples incubation for 10 min at 72°C.

Presented relative analysed genes' expression levels were calculated using $2^{-\Delta\Delta Ct}$ method. Results were normalized according to expression of glyceraldehyde-3-phosphate dehydrogenase (GAPDH) gene and undifferentiated cells, seeded on standard tissue culture plate surface (TCPS) at initial time point, genes expression.

Table 2.2. Sequences of analysed genes primers pairs, used for qPCR.

Gene	Primer
OPN	FW: 5‘-CCAGCCAAGGACCAACTACA-3‘
	RV: 5‘-TGGCTACAGCATCTGAGTGTTT-3‘
OCN	FW: 5‘-TGCATTCTGCCTCTCTGACC-3‘
	RV: 5‘-CTGGGGCTCCAAGTCCATTG-3‘
Runx2	FW: 5‘-TGAGATTTGTAGGCCGGAGC-3‘
	RV: 5‘-GCTTCTGTCTGTGCCTTCTTG-3’
GAPDH	FW: 5‘-AGTGCCAGCCTCGTCTCATA-3‘
	RV: 5‘-ATGAAGGGGTCGTTGATGGC-3‘

2.2.5.5 Mineralization assay

ARS staining was performed in order to evaluate calcium-rich deposits in cell cultures. Briefly, after predetermined time points OM/GM was removed. Afterwards, cells were rinsed 2x with PBS and fixed with 4% paraformaldehyde at room temperature for 15 min with gentle shaking (25 rpm). Fixative residues were removed and cells were washed with PBS. ARS dye solution (pH = 4,1–4,3) was added and incubated at room temperature for 20 min with shaking (25 rpm). Thereafter, ARS solution was discarded; samples were rinsed three times with deionized water and centrifuged at 100g for 30 s (HERMLE Labortechnik GmbH).

For qualitative differentiation evaluation, samples were analysed microscopically (Olympus IX51). Monolayer appeared red/brownish when stained.

For quantitative evaluation, ARS were dissolved in 5% perchloric acid; after 10 min, absorbance was measured at 490 nm using a microplate spectrophotometer Varioskan Flash (Thermo Scientific). As a background value, scaffolds without cells were used.

2.2.5.6 Statistical analysis

R program package (RStudio v1.1.442) was used to perform statistical analysis. The qPCR results were analysed with Rotor-Gene 6000 Series Software 1.7 and R.

Data were reported as median ± IQR (of at least 3 independent experiments, $N \geq 3$ samples per group). The number of FA within cells is presented with distribution density function. Data normality was evaluated using Shapiro-Wilk test (when $n \geq 5$). Significant differences of not normally distributed results, between three and more groups were evaluated by Kruskal–Wallis one-way analysis of

variance test; post hoc Tukey test was used to highlight differences in data. Normally distributed data (also, when $n < 5$) with three and more groups was evaluated using a one-way analysis of variance (ANOVA) and subsequently analysed with the post hoc Tukey test. p-values < 0.05 were considered to be statistically significant.

3. RESULTS AND DISCUSSION

Tissue engineering is an interdisciplinary branch of science combining principles of engineering and life sciences to create artificial constructs which could repair and reinforce functions of damaged or deseased tissue (Castells-Sala Cristina, Alemany-Ribes Mireia, 2015; Howard et al., 2008). In the construction of artificial tissue it is important to ensure interaction between three main components of tissue engineering – cells, scaffolds and bioactive molecules. Only properly selected cells, scaffolds, and bioactive molecules are able to produce a construct capable of efficiently regenerate damaged tissue (Murphy et al., 2013). It is known that the substrate a cell interacts with has a major impact on cell fate (Urrutia et al., 2017). Therefore, in artificial tissue construct production, there is an aim to create scaffolds that only by their structure and composition would ensure optimal stem cell proliferation, migration, and differentiation (Krishna et al., 2016).

This work was dedicated to the development of artificial bone tissue. Here we analysed adult stem cells, extracted from dental pulp, interaction with different substrates. Changes in the properties of cells depending on substrate surface geometry, chemical composition and protein coating were analyzed. Also, using *in vitro* assays, evaluating the potential response of the organism to the different constructs which could be used in damaged bone treatment was attempted.

Mesenchymal DPSC extracted from rat dental pulp was selected as the study model. These cells are easily accessible, multipotential, and therefore excellent for tissue engineering applications and research (Mori et al., 2011; Pierdomenico et al., 2005). Our results confirmed their ability to easily differentiate into adipocytes, myocytes, and osteoblasts. Therefore their multipotency capabilities are the same as bone marrow-derived mesenchymal stem cells, which are extensively used in tissue engineering studies (Tamaki et al., 2013). It is known that mesenchymal stem cells isolated from different tissues might demonstrate tendency to spontaneously differentiate into the same tissue cells (Naruse et al., 2004). Thus, growing DPSC on specific substrates their spontaneous osteogenic differentiation could be achieved (Du et al., 2019). Considering the good characteristics of DPSCs and their relatively easy extraction procedure, which does not require additional intervention into the patient's organism, it can be stated that these cells might be successfully used for artificial bone tissue construction.

3.1 Influence of substrate topography on cell behaviour

It is well known, that cell-surrounding environment plays an important role in various cell processes (Murphy et al., 2013; Tavakol et al., 2013; Kajita et al., 2010). It was shown that scaffold micro- and nano- topographies alter cellular cytoskeletal remodelling, focal adhesion formation, and various signalling pathways activation, which in turn affects cell fate (proliferation, migration, differentiation etc.) (Zhang et al., 2018; Zhu et al., 2018; Niu et al., 2017; Yao et al., 2017; Kim et al., 2016; Abagnale et al., 2015; Chaubey et al., 2008; Hamilton et al., 2008; Deligianni et al., 2001). However, the manufacture of micro- and nano-structured surfaces is time-consuming, expensive and requires high precision.

These production problems could be solved with 3D printing, which ensures fast and inexpensive manufacture of highly reproducible, controlled geometry, interconnected porosity and patient specific scaffolds for bone tissue engineering. Despite these 3D printing advantages, only macrosurface (> 100 µm) topographies could be produced using this technology (Shanjani et al., 2011; Klammert et al., 2010; Leukers et al., 2005; Lam et al., 2002). However, little is known about macrostructured pattern impact on stem cell fate. For this purpose, we evaluated the impact of 3D PLA surface macrotopography on rat's DPSC orientation and morphology, leading to a different cell behavior.

3.1.1 Manufacture of PLA scaffolds with different surface topographies

In surface topography studies, two different scaffolds with wavy and woodpile porous macrostructures (>100 µm) were designed and 3D printed. Produced wavy scaffolds' structure was composed of 188 µm PLA filaments moulded together and forming a plain wavy macro-structure (Fig. 3.1 A). Meanwhile, in porous scaffolds, 500 µm threads formed 300 µm size holes, which taken together formed 50 % porosity (Fig. 3.1 B). In addition, specified pore size is the most appropriate for bone tissue regeneration *in vivo* (Hannink and Arts, 2011; Karageorgiou and Kaplan, 2005) probably because same or even higher porosity facilitates the nutrition metabolism in the tissue and, as a consequence, it is typical for a natural bone ECM (Wall and Board, 2014).

The tissue culture plate surface (TCPS) was used as the control for this part of experiments.

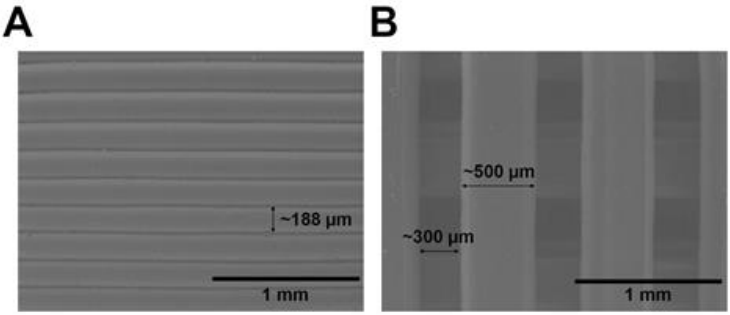

Figure 3.1. The SEM images of the 3D printed PLA scaffolds. A - 2.5D full-filled wavy scaffold; diameter of PLA filament is approximately 188 µm; B – 3D porous PLA scaffold; diameter of the filament – 500 µm; pore size is approx. 300 µm.

3.1.2 Effect of PLA scaffold topography on DPSC morphology and proliferation

Results revealed that tested PLA macrotopographies influenced different DPSC orientation and morphology: wavy surface determined more straightened morphology of cells, meanwhile, DPSC seeded on porous scaffold were flatter and bent over on the PLA filament (Fig. 3.2). The influence of such topography on DPSC morphology was confirmed by determining aspect ratio of cell dimensions (Fig. 3.3 A). Evidently, cells on wavy scaffolds were much more straightened, extended and stretched out compared to cells which were grown on porous and TCSP surfaces ($p<0.001$). Furthermore, DPSC nucleus morphology was evaluated by measuring its aspect ratios (Fig. 3.3 B). It was revealed that cells grown on all tested macrostructured surfaces had differently shaped nucleus ($p<0.001$): nucleus of DPSC grown on porous scaffolds had the roundest shape, while plate surface promoted the largest nucleus elongation.

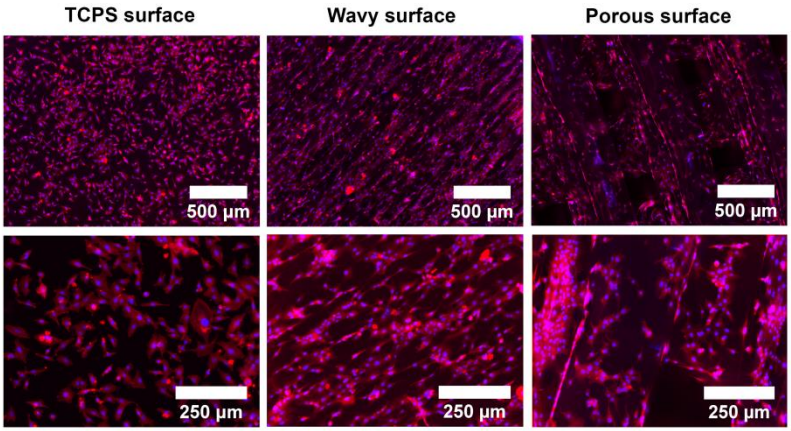

Figure 3.2. Differently structured porous and wavy PLA scaffolds dependent DPSC morphology. Immunocytochemical visualization of cell F-actin filaments (red color, stained with Rhodamine Phalloidin) and nuclei (blue color, stained with DAPI) Surface of tissue culture plate (TCSP) was used as a control.

Previously it was thought that only micro- and nano- structures can influence cell morphology (Zhang et al., 2018; Zhu et al., 2018; Abagnale et al., 2015; 2017; Niu et al., 2017; Yao et al., 2017; Kim et al., 2016; Yim et al., 2007). Therefore, our results imply that surface pattern in the scale of >100 µm still alters cell shape and induces different ECM tensions which undoubtedly affect cell fate.

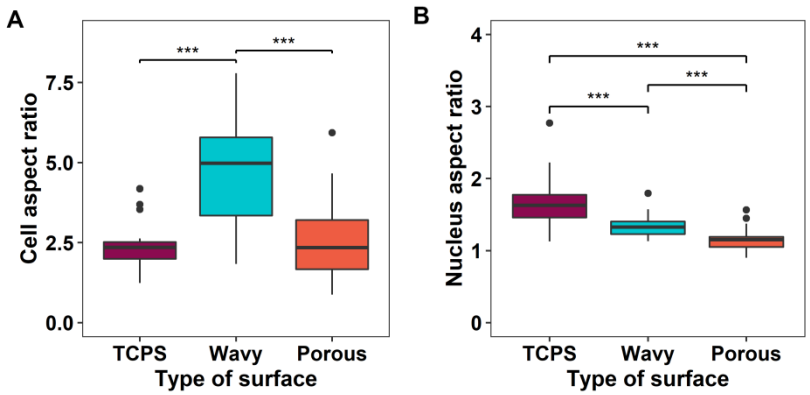

Figure 3.3. DPSC and their nucleus morphology changes. A - aspect ratio of cells; B – aspect ratio of cell nucleus. Surface of tissue culture plate (TCSP) was used as a control. Results are presented as median ± IQR (of at least 3 independent experiments, N ≥ 3 samples per group). Statistically significant data are indicated as *** ($p < 0.001$).

After DPSC proliferation analysis differences between cell counts determined on porous and wavy scaffolds were not registered (Fig. 3.4). Even so, obtained results showed greater DPSC proliferation on both studied PLA scaffolds versus control TCPS surface: within 120 h, number of cells on TCPS surface increased about 8 times, which is lower than cell number on wavy (about 12 times, $p < 0.05$) and on porous PLA scaffolds (about 14 times, $p < 0.01$). These differences could have appeared due to surface spatial structure (2,5- 3D) which tends to increase the proliferation of various cell lines (Zhu et al., 2015; Bhat and Kumar, 2012; Saşmazel et al., 2008).

Apart from apparent difference in surface area that occurs in 3D structures versus 2D, other aspects, such as surface roughness, shape, and diameter, should also be considered. Different components of the surrounding environment of the cell preferentially interact with certain integrin family members which are able to feel and react to the surface transmitting signals to the nucleus. In our study, DPSCs

grown on woodpile macrosurfaces of porous scaffolds and in macrogrooves of wavy scaffolds displayed different cytoskeletal arrangement, which revealed as different cell stretching and compression, likely enhanced DPSC proliferation compared to planar surface. Literature data implies that curved cell bears greater in-plane tensile forces, linking membrane curvature to increased cytoskeletal contractility, which results in activation of YAP signalling pathway. This signalling cascade plays a role in cell migration, proliferation and survival (Mascharak et al., 2017; Abagnale et al., 2015).

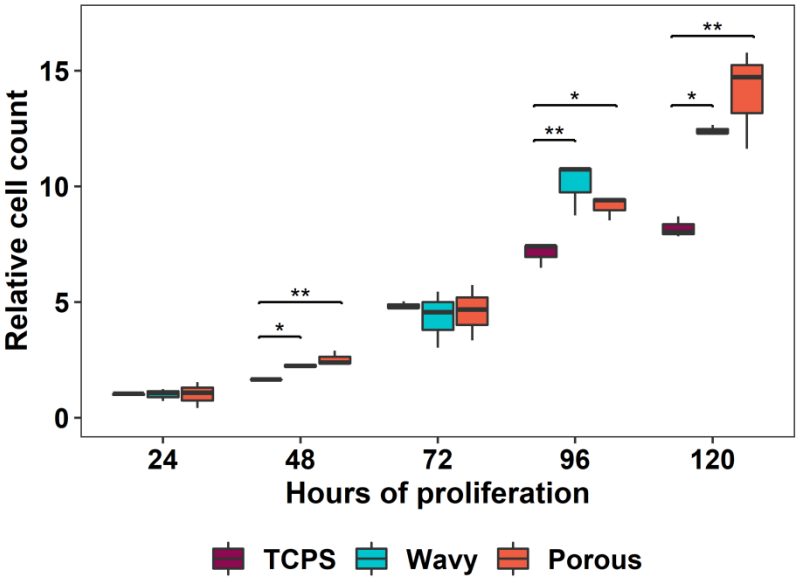

Figure 3.4. Differently structured porous and wavy PLA scaffolds dependent DPSC proliferation. Results were standardized according to the cell numbers determined on the appropriate surface after 24 h of incubation. Results are presented as median ± IQR (of at least 3 independent experiments, N ≥ 3 samples per group). Statistically significant data are indicated as „*" when $p<0.05$ and „**", kai $p < 0.01$.

3.1.3 Effect of surface macrotopography on DPSC osteogenic differentiation

To evaluate whether PLA scaffold's macrotopography is sufficient enough to induce DPSC spontaneous osteogenesis, cells were seeded on tested substrates and the early (Runx2 and OPN protein gene expression) and late (ALP activity, ECM mineralization and OCN protein gene expression) bone formation markers were analysed (Chen et al., 2018b; Xu et al., 2015; Mihaila et al., 2014; Roberts et al., 2011; Huang et al., 2007; Lian et al., 1993). Since osteogenesis is a stepwise process, therefore, the obtained results were discussed according to this process order in the organism.

Runx2 and OPN proteins' genes expression levels were evaluated by qPCR (Fig. 3.5). Data were normalized according to expression of glyceraldehyde-3-phosphate dehydrogenase (GAPDH) gene and expression of genes in undifferentiated cells, grown on the TCPS at initial time point. Results showed that both wavy and porous PLA macrostructured surfaces stimulated spontaneous DPSC differentiation towards osteogenic lineage by upregulating Runx2 and OPN genes expression. The highest Runx2 gene expression was detected at the beginning of spontaneous differentiation; in DPSC grown on wavy scaffolds it increased greater ($p < 0.01$) compared to porous scaffolds. In subsequent differentiation days, significant downregulation in Runx2 gene expression was observed on both PLA surfaces, however, statistically significant changes in Runx2 gene expression between different tested scaffolds were not observed. OPN gene expression during spontaneous differentiation statistically significantly increased in time-dependent manner throughout predetermined time points on both, wavy and porous, macrostructured PLA scaffolds. In addition, after 1 and 7 days of spontaneous differentiation, differences in OPN gene expression levels ($p < 0.05$) between wavy and porous scaffolds were observed.

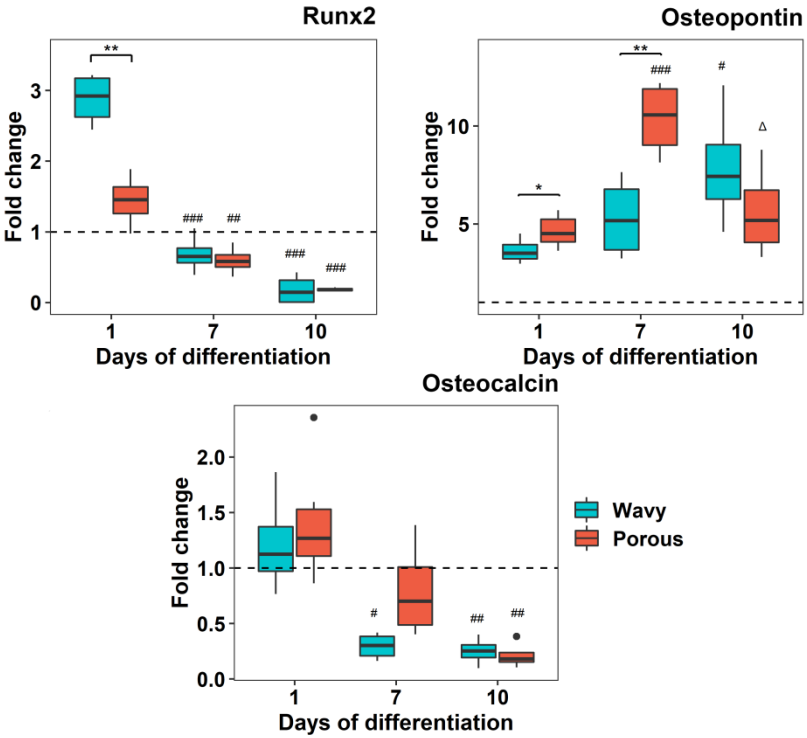

Figure 3.5. Osteogenic-related proteins (Runx2, OPN, OCN) genes expression levels in DPSC seeded on wavy and porous PLA scaffolds after spontaneous osteogenic differentiation. Results are presented as median ± IQR. Statistically significant differences between cells grown on porous and wavy scaffolds are marked with * ($p < 0.05$) and ** ($p < 0.01$), while # shows statistically significant differences compared to day 0 within the same scaffold group (wavy or porous) – # ($p < 0.05$), ## ($p < 0.01$), ### ($p < 0.001$) and Δ demonstrates a significant differences compared to day 7 within the same scaffold group – Δ ($p < 0.05$).

ALP activity results indicated that after 10 days of differentiation, ALP activity in DPSC grown on both PLA macro-structured scaffolds was statistically significantly increased compared to DPSC at 0^{th} and 7^{th} days of differentiation (Fig. 3.6 C). Not to mention, after the 10 days of differentiation the highest ($p < 0.07$) ALP activity was detected in cells grown on porous PLA scaffolds compared to DPSC grown on the wavy ones.

Spontaneous osteogenic differentiation was also evaluated by ARS staining. It was observed that cells formed groups on PLA scaffolds macrogrooves and macrocavities, where the ECM mineralization was extremely pronounced (Fig. 3.6 A). Quantitative evaluation of ECM mineralization (Fig. 3.6 B) showed that even after 7 days of spontaneous differentiation calcium accumulation was significantly increased on both macrostructured PLA scaffolds. In addition, a higher calcium deposition in ECM was elucidated on porous scaffolds ($p < 0.05$) at day 7^{th}; furthermore, this difference remained in later differentiation days ($p < 0.05$).

In contrast to other analysed osteogenesis markers, OCN showed a slightly continuous decrease in gene expression levels from the very beginning of differentiation on both surfaces (Fig. 3.5). OCN is an ECM protein that is a specific marker for mature osteoblasts. Most likely, during our experiment, DPSC did not have enough time to reach the late stage of osteogenic differentiation, to completely differentiate into osteoblasts (Huang et al., 2007).

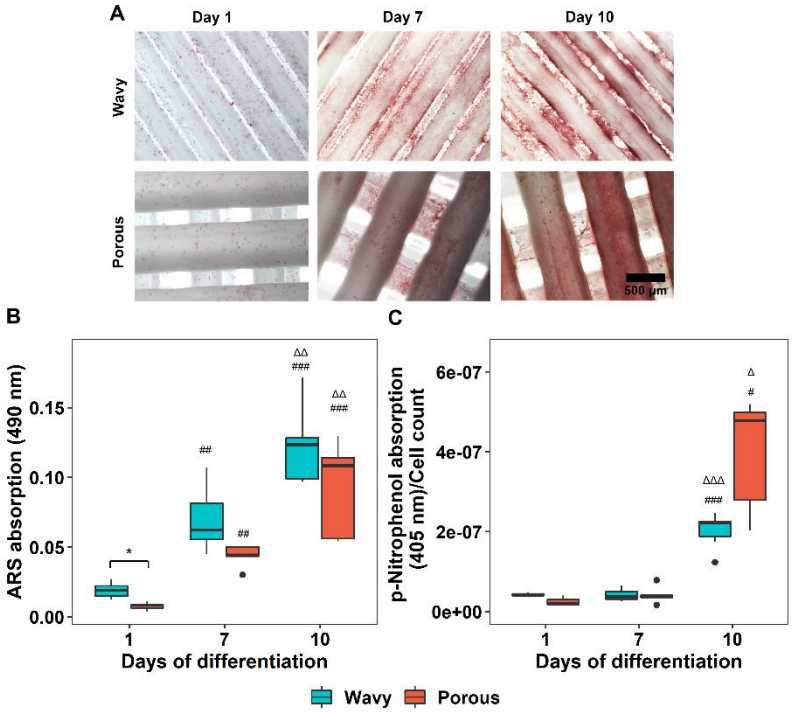

Figure 3.6. Spontaneous osteogenic differentiation assessment. A - qualitative ECM mineralization analysis by ARS staining; B - quantification of ECM mineralization by measuring the absorption of dissolved ARS; C – ALP activity evaluated by p-nitro phenol assay; obtained results were standardized according to the cell numbers determined on the appropriate surface after predetermined time points. Results are presented as median ± IQR. Statistically significant differences between cells grown on porous and wavy scaffolds are marked with * ($p < 0.05$), while # shows statistically significant differences compared to day 0 within the same scaffold group (wavy or porous) – # ($p < 0.05$), ## ($p < 0.01$), ### ($p < 0.001$) and Δ demonstrates a significant differences compared to day 7 within the same scaffold group – Δ ($p < 0.05$), ΔΔ ($p < 0.01$), ΔΔΔ ($p < 0.001$).

Thus, both surface macrotopographies had almost similar positive impact on DPSC osteogenic differentiation potential and one of the main factors determining cell osteogenic commitment could be cell shape and cytoskeletal arrangement generated by the contact of cell and surface macrostructures. Current knowledge states that only micro- or nano- grooves and woodpile shapes elevate cytoskeletal tension which, in turn, tends to activate signalling pathways, which are important in osteogenesis (Kilian et al., 2010; McBeath et al., 2004).

In addition, spontaneous osteogenic differentiation results revealed that even without additional osteogenic inducers (dexamethasone, ascorbic acid and ß-glycerophosphate) the osteogenic-related genes expression (Runx2 and OPN), ALP activity and ECM mineralization were increasing during experimental time in DPSC grown on macrostructured PLA scaffolds. Accordingly, it can be stated that supplementing factors for DPSC osteogenic differentiation is unnecessary, and osteogenic differentiation does not require the precise micro- or nano-structured scaffold.

3.2 Influence of substrate chemical composition on cell behavior

Composite PLA+HA and PLA+BG scaffolds (Fig. 3.7) were used to evaluate the influence of substrate chemical composition on DPSC fate. Composites made of PLA polymer and HA or BG bioceramics were not chosen randomly, in order to apply obtained results in artificial bone tissue creation.

One of the promising artificial bone graft manufacture techniques is 3D printing and, considering potential chemical constitution, composite material (Burgio et al., 2018; Huang et al., 2018a; Kuss et al., 2018; Qi et al., 2018; Kim et al., 2017; Zhang et al., 2016). 3D printing suitable composites are commonly developed by mixing HA

and BG bioceramics with PLA or PCL polymers. Addition of bioceramics to the polymer improves its biocompatibility, osteoconductivity and even osteo- or angio-inductivity (Motealleh et al., 2017; Zhang et al., 2016). However, there are no studies in which osteoconductive and osteoinductive properties of HA or BG and PLA composites scaffolds fabricated using 3D printing technique would be compared to each other. Thus, to determine, which composite material (PLA+HA or PLA+BG) is the most suitable for the use in artificial bone grafts production by 3D printing technology, their effect on DPSCs adhesion, migration, proliferation and osteogenesis were compared.

Based on surface topography results, which revealed that both investigated macrogeometries had similar positive effect on DPSC osteogenesis, we developed an improved macrostructured interconnected porosity scaffold model, which was used for the production of composite scaffolds. In order to maintain the positive osteoinductive properties of waves and pores, each scaffold layer consists of two 400 μm width and 200 μm height threads moulded together, which formed a 400 μm height layer. All scaffolds had eight layers. Scaffold geometry was retained, the same as in the case of macrotopographic samples, except that threads were rotated at an angle of 60° in respect to the ones of the previous layer.

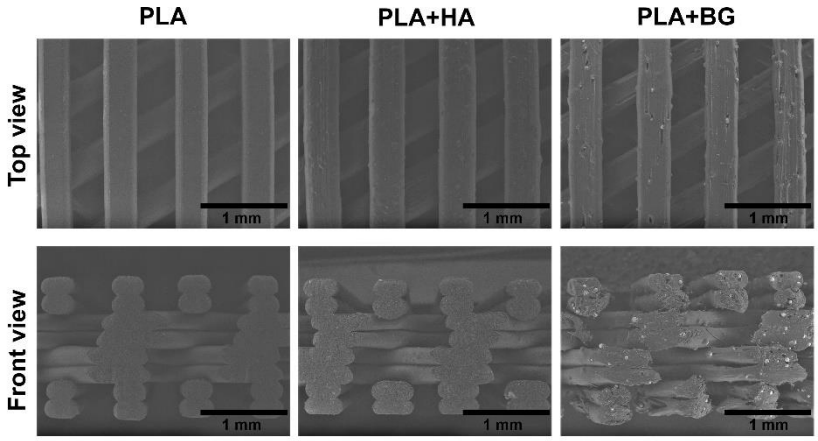

Figure 3.7. The SEM images of the 3D printed composite scaffolds. Diameter of the filament is approx. 400 μm; pore size is approx. 400 μm.

3.2.1 Effect of composite PLA scaffolds on cell adhesion

Attachment to the substrate is essential for successful cell proliferation and differentiation (Di Benedetto et al., 2015). To compare the impact of bioceramic-polymer composites on DPSCs adhesion efficiency, the cells were seeded on the tested composite scaffolds and cell surface area (0.5, 2 and 24 h post-seeding) was analysed by visualising DPSC F-actin filaments.

Obtained cell surface area measurements (Fig. 3.8 B) showed that DPSCs were capable to adhere to all the tested surfaces. However, after 0.5 h, the cells adhere better to composite PLA+HA and PLA+BG scaffolds compared with pure PLA ($p<0.01$ and $p<0.05$ respectively). Although, after 24 h the best DPSCs adhesion efficiency was observed on PLA scaffolds and the worst adhesion was determined on PLA+BG, compared with pure PLA ($p<0.01$) and PLA+HA ($p<0.001$).

To understand better the cell adhesion process, focal adhesion spots (24 h post-seeding) within the cell were visualised (Fig. 3.8 A) and quantified (Fig. 3.8 C). The results showed that the minimum number of FA were formed in the cells grown on composite PLA+BG scaffolds, which means that DPSCs adhesion strength on PLA+BG scaffolds was the weakest compared with PLA+HA ($p<0.05$) and pure PLA ($p<0.05$). It is known that cells can only attach to surfaces containing deposited proteins from the medium or body fluids. The interaction between proteins and PLA+HA or PLA+BG surface is primarily facilitated by coordinate covalent and electrostatic bonds. For example, electrostatic interactions could occur between the negatively charged ions (in BG) or phosphorus groups (in HA) surface and protonated amine groups (–NH:) of proteins, thus high surface charge density of the ions or phosphorus of BG and HA surfaces induce strong protein adsorption (Srinivasan et al., 2012; Lobel and Hench, 1996; Gorbunoff and Timasheff, 1984). Thus, BG containing scaffolds should have better or at least the same interaction with cells as pure PLA scaffolds. However, in our study, the BG beads had a negative effect on cell attachment in the first 24 hours of cell incubation onto the surfaces.

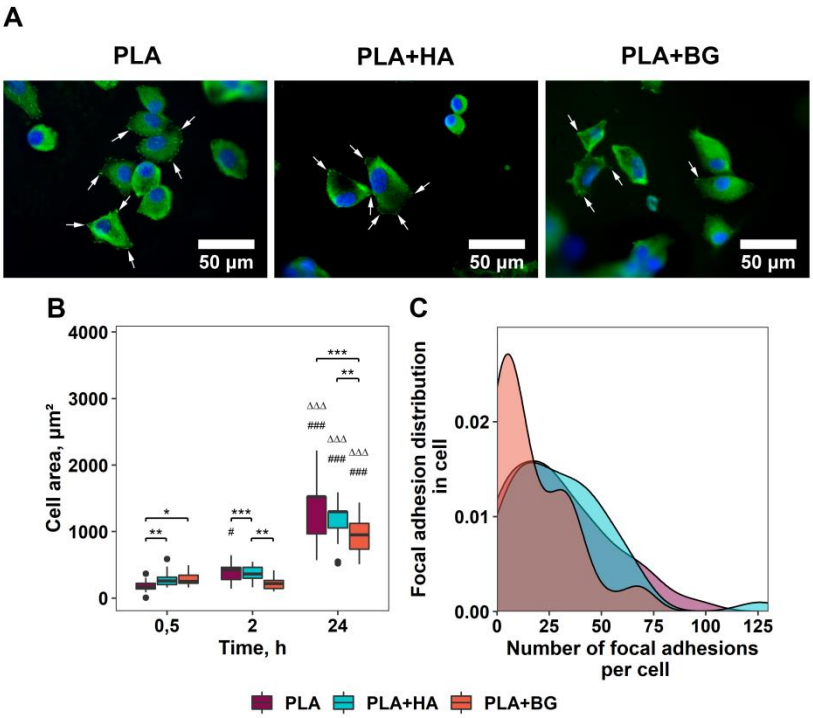

Figure 3.8. DPSC adhesion on 3D printed composite scaffolds. A – immunofluorescence staining of nucleus (blue color, DAPI) and FA spots (green color, vinculin) in DPSCs, 24 h post-seeding; B – cell surface area after culturing for 0.5, 2 and 24 h on the scaffolds; C – quantitative FA evaluation within the cells after culturing for 24 h. Statistically significant data between different scaffold groups are indicated as * ($p < 0.05$), ** ($p < 0.01$) and *** ($p < 0.001$), while # shows statistically significant differences compared to 0.5 h within the same scaffold group – # ($p < 0.05$), ### ($p < 0.001$), Δ demonstrates significant differences compared to 2 h within the same scaffold group –ΔΔΔ ($p < 0.001$).

3.2.2 Influence of composites on cell migration and proliferation

Substrate chemical composition can act as a chemoattractant for cell migration as well as initiate their proliferation (Tamburaci and Tihminlioglu, 2018; Anselme, 2000). These surface features are very important in tissue engineering. In order to achieve successful tissue regeneration, after construct implantation, the stem cells surrounding the damaged tissue area must migrate there. In the damaged area stem cells should proliferate, differentiate and synthesise tissue specific ECM. This would gradually replace the artificial construct with a fully functional, newly formed tissue (Su et al., 2018). Therefore, a scaffold developed for bone regeneration must also be attractive for cell migration and proliferation (Su et al., 2018; Ohashi et al., 2017).

To evaluate the impact of the different chemical composition of scaffold filaments on cell attraction, vertical migration of DPSCs onto tested scaffolds was assessed (Fig. 3.9 A). The results indicated that among the tested scaffolds the most attractive for cells was composite PLA+BG surface, in this case, DPSCs demonstrated the highest migration potential compared to PLA ($p < 0.01$) and PLA+HA ($p < 0.01$). These results can be caused by dissolved ions from 45S5 BG, which stimulate cell migration (Li et al., 2016; Yu et al., 2016). The better DPSC migration onto PLA+BG scaffolds could also explain the worst cell adhesion on this type of surface. Intermediate level of attachment strength produces maximal migration rates (DiMilla et al., 1991). At low adhesive strength sufficient traction cannot be generated for cell migration to proceed, whereas, at higher adhesive strength, the cells do not release their adhesions efficiently (Huttenlocher et al., 1995). Thus, this explains why DPSCs have formed a smaller amount of FAs compared to PLA+HA scaffolds.

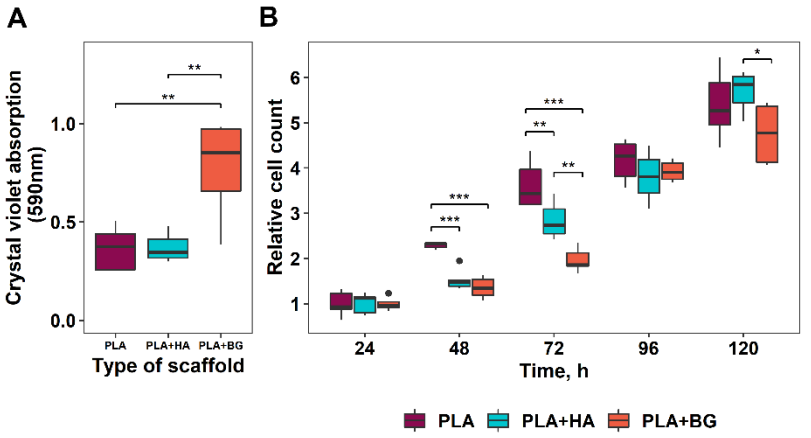

Figure 3.9. DPSC migration and proliferation on composite scaffolds. A – evaluation of vertical cell migration onto the composite scaffolds using crystal violet assay; B – relative DPSC proliferation rate; data is standardized according to the number of cells maintained on appropriate scaffolds for 24 h. Results are presented as median ± IQR. Statistically significant results indicated as * ($p<0.05$), ** ($p<0.01$) and *** ($p<0.001$).

The assessment of cell proliferation activity indicated that, almost after all time measurements, DPSCs showed significantly better proliferative activity on pure PLA scaffolds compared to composite ones (Fig. 3.9 B). The worst DPSC proliferation was registered on the composite PLA+BG scaffolds. However, after 96 and 120 h, significant differences between PLA and PLA+HA or PLA+BG scaffolds were not detected. Such slower cell proliferation could be associated with the onset of DPSC osteogenic differentiation on these composite scaffolds. It is well known that stem cells committed to differentiate into the specific lineage exit the cell cycle and start the differentiation process within the cell (Rutkovskiy et al., 2016; Li and Kirschner, 2014; Cooper, 2000; Janners and Searls, 1970).

3.2.3 Effects of composites on osteogenic cell differentiation

To prove that slower DPSCs proliferation on composite scaffolds was determined by induction of osteogenic processes within the cells, the effect of scaffolds' chemical composition on DPSC osteogenesis was evaluated. In order to compare which of the bioceramics (HA or BG) demonstrates better osteoinductivity properties, ALP activity, osteogenesis-related gene expression and bone tissue specific ECM were analysed in DPSCs cultivated on PLA+HA as well as PLA+BG composite scaffolds. The obtained results were discussed sequentially, according to osteogenesis process order in the organism (Burr and Allen, 2014).

Runx2 and OPN proteins gene expression measurement results showed that all tested scaffolds stimulated DPSC differentiation towards osteogenic lineage by upregulation of proteins Runx2 and OPN gene expression (Fig. 3.10) (data were normalized as in case of surface topography experiments). Moreover, the highest Runx2 protein gene expression was determined in cells maintained on all tested scaffolds at 10th day of differentiation. In DPSCs grown on PLA+BG, it tended to increase greater compared to cells grown on pure PLA ($p<0.27$) and PLA+HA ($p<0.09$) scaffolds. However, in this case, differences in Runx2 gene expression did not reach statistically significant levels. In the case of OPN gene expression, it remained almost unchanged at 1st and 7th differentiation evaluation days in cells grown on all investigated scaffolds. Enhanced OPN expression after 10 days of culture was observed in cells maintained on PLA+BG scaffolds ($p<0.01$) compared to PLA and PLA+HA groups (Fig. 3.10).

ALP activity results indicated that in DPSCs grown on composite PLA+BG scaffolds enzyme activity was increased even after 1st cultivation day, compared to pure PLA ($p<0.01$) and PLA+HA ($p<0.01$) (Fig. 3.11 A). Later on, ALP activity in DPSCs grown on

PLA+BG scaffolds gradually decreased. However, the highest enzyme activity, in the cells maintained on PLA and PLA+HA scaffolds, was detected only after 10 days of differentiation (Fig. 3.11 A).

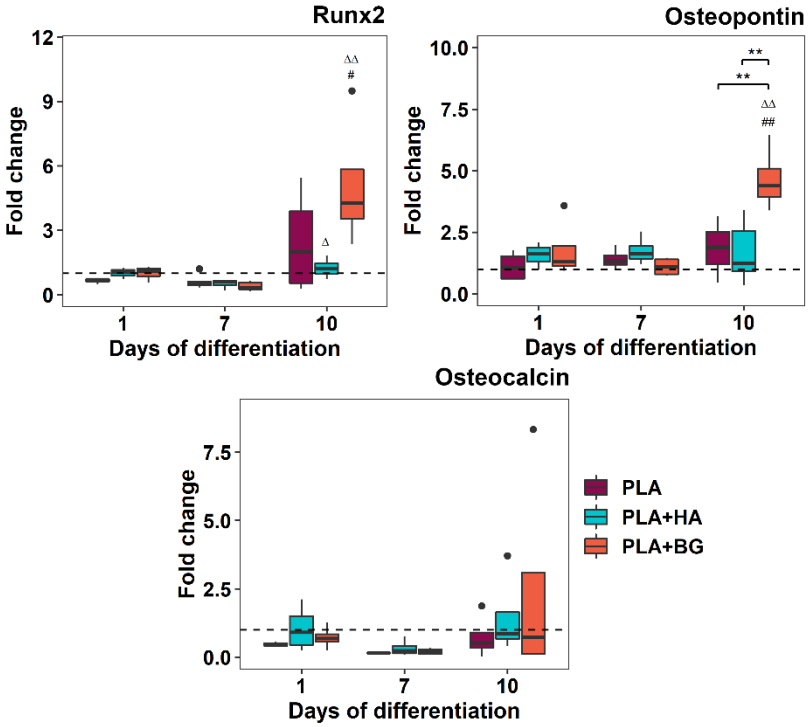

Figure 3.10. Osteogenesis-related proteins (Runx2, OPN, OCN) genes expression levels in DPSC grown on 3D printed composite scaffolds. Results are presented as median ± IQR Statistically significant differences between cells grown on different scaffolds groups are marked with ** ($p<0.01$), while # shows statistically significant differences compared to day 1 within the same scaffold group – # ($p<0.05$), ## ($p<0.01$), Δ demonstrates a significant differences compared to day 7 within the same scaffold group – ΔΔ ($p<0.01$).

Bone tissue specific ECM analysis revealed that DPSCs grown on all surfaces tended to accumulate collagen in their ECM, however, significant differences between scaffold impact on collagen accumulation were not observed (Fig. 3.11 B). In contrast, ECM mineralisation results indicated that even at the 1st day of DPSC cultivation on tested scaffolds, higher calcium depositions were observed on both composite scaffolds (PLA+HA ($p<0.001$) and PLA+BG ($p<0.001$)) compared to pure PLA (Fig. 3.14 C). Moreover, at 7th and 10th day of the differentiation, the greatest and statistically significant increase of ECM mineralisation was registered in cell cultures maintained on composite PLA+BG scaffolds.

Unlike other bone formation markers, differences in OCN gene expression were not observed at any time point in cells grown on tested scaffolds (Fig. 3.10). Most likely, as in case of substrate topography experiments, DPSCs did not have enough time to reach the late stage of osteogenic differentiation and thus completely differentiate into osteoblasts (Huang et al., 2007).

Both PLA+HA and PLA+BS composites initiate spontaneous DPSC osteogenesis. However, PLA+BG scaffolds demonstrated the strongest osteoinductivity. We believe that these results may be determined by chemical composition of the BG particles. Studies have shown that during BG degradation, the calcium, phosphorus, and silicon ions are released, which further stimulate stem cell metabolic activity, proliferation, and osteogenesis (Qi et al., 2018; Valerio et al., 2004; Silver et al., 2001; Xynos et al., 2001).

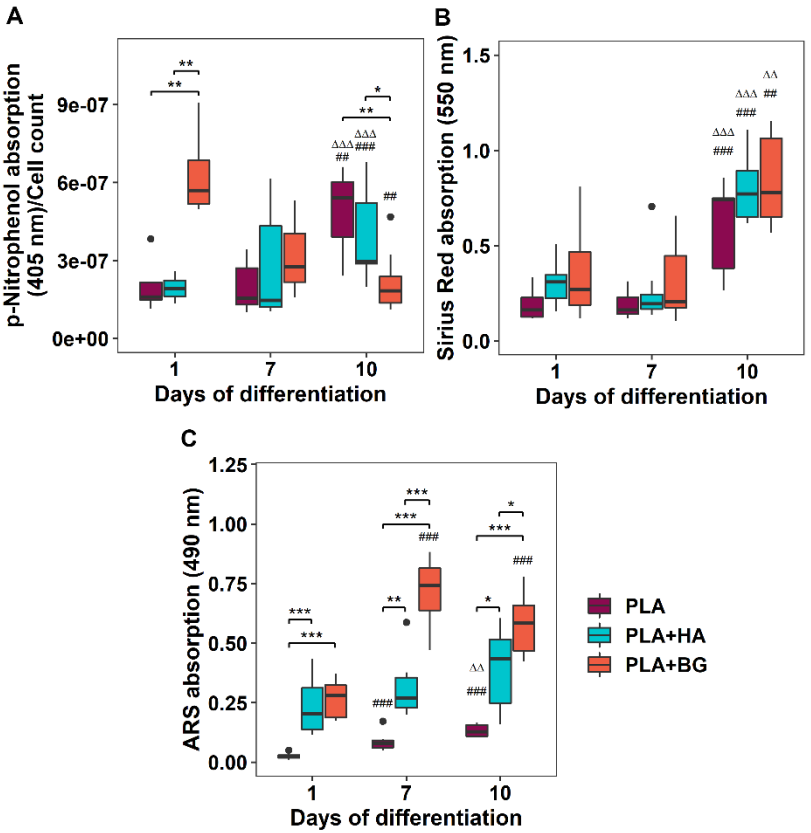

Figure 3.11. Osteogenic differentiation assessment. A – ALP activity evaluated by p-nitrophenol assay; B – DPSCs collagen production evaluated by Sirius Red staining; C – ECM mineralization analysis by ARS staining. Results are presented as median ± IQR. Statistically significant differences between different scaffolds groups are marked with * ($p<0.05$), ** ($p<0.01$) and *** ($p<0.001$), while # shows statistically significant differences compared to day 1 within the same scaffold group – ## ($p<0.01$), ### ($p<0.001$), Δ demonstrates significant differences compared to day 7 within the same scaffold group - ΔΔ ($p<0.01$), ΔΔΔ ($p<0.001$).

3.3 Influence of ECM proteins on cell fate

Protein-coated surfaces modulate cell fate (Li et al., 2019; Salvay et al., 2008). Therefore, scaffolds produced for artificial tissue construction are usually supplemented by decoration with various proteins (collagen, elastin etc.) and signalling molecules (melatonin, RGD sequences etc.) (Miao et al., 2019; Soriente et al., 2018; Vila et al., 2016). A new method of scaffold decoration was tested in this work – surface coating with cell-derived ECM. Such ECM has more complex structure compared to single proteins or signalling molecules, thus it is able to provide more effective regeneration of damaged tissue (Kim et al., 2018; 2019).

Scaffold coating with cell derived ECM is a rapidly growing field of research. In the production of artificial bone tissue constructs, such ECM is used to decorate various polymer (PCL, PLGA), composites (PCL+PLGA+TCP etc.) or bioceramic (HA, biphasic calcium phosphate etc.) scaffolds, which are produced by FFF 3D printing, electrospinning or similar methods (Burgio et al., 2018; Kim et al., 2018; Kumar et al., 2016; Noh et al., 2016; Pati et al., 2015; Liao et al., 2010b; 2010a). 3D printing is considered to be one of the most promising artificial bone graft manufacture techniques where potential scaffold chemical constitution is PLA-bioceramic composite material. (Burgio et al., 2018; Huang et al., 2018a; Kuss et al., 2018; Scaffaro et al., 2016). Therefore, constructs made of 3D printed composite material and decorated with cell-derived ECM, are expected to be relatively inexpensive scaffolds for bone regeneration, demonstrating good osteo- and angio- induction properties. Despite that much research has been done in this field, PLA scaffolds, produced with FFF method and coated with cell derived ECM, impact on cell fate is still not elucidated. Moreover, in previous studies, only primary BMSC or osteoblast cell line-formed ECM effect on cell behaviour was evaluated. (Burgio et al., 2018; Kim et

al., 2018; Liao et al., 2010b; 2010a). However, BMSC extraction procedure is complicated and painful for the patient (Tamaki et al., 2013), thus attempts are being made to proceed to clinical trials using other types of adult stem cells, such as DPSC (Mori et al., 2011; Pierdomenico et al., 2005). Therefore, to apply DPSC-formed-ECM-coated scaffolds for bone regeneration, it is important to elucidate the effect of such ECM on cell fate. For this reason, DPSCs were grown on FFF 3D printed porous PLA scaffolds for 7 days. After predetermined time, samples were decellularized, then DPSC were re-seeded on freshly obtained decellularized scaffolds (PLA+ECM) and cell behaviour as well as their osteogenesis were analysed.

3.3.1 Effect of cell-derived ECM coated scaffolds on cell adhesion

As mentioned earlier, attachment of the cell to the surface is a very important process that can determine cell fate (Di Benedetto et al., 2015). Therefore, the impact of ECM proteins on DPSC adhesion efficiency was evaluated. Thus, the DPSCs were seeded on PLA and PLA+ECM scaffolds and cell surface area (0.5, 2 and 24 h post-seeding) was analysed by visualising DPSC F-actin filaments. Obtained F-actin filaments fluorescent microscope images (Fig. S3) and cell surface area measurements (Fig. 3.12 B) showed that after all analysed time intervals (0.5, 2 and 24 h post-seeding) cells attached better to ECM coated scaffolds, correspondingly larger DPSC surface areas were determined on PLA+ECM samples compared to pure PLA scaffolds ($p < 0.001$).

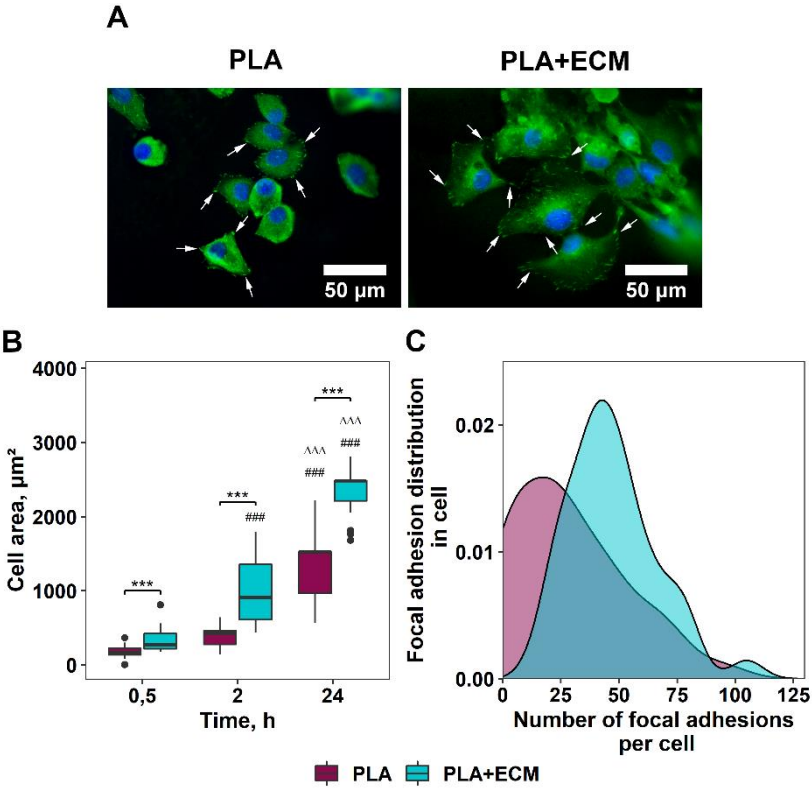

Figure 3.12. DPSC adhesion on ECM coated scaffolds. A – immunofluorescence staining of nucleus (blue color, DAPI) and FA spots (green color, vinculin) in DPSCs, 24 h post-seeding; B – cell surface area after culturing for 0.5, 2 and 24 h on the scaffolds; C – quantitative FA evaluation within the cells after culturing for 24 h. Statistically significant data between different scaffold groups are indicated as *** ($p < 0.001$), while # shows statistically significant differences compared to 0.5 h within the same scaffold group – ### ($p < 0.001$), Δ demonstrates significant differences compared to 2 h within the same scaffold group – ΔΔΔ ($p < 0.001$).

To understand DPSC-formed ECM influence on cell attachment process better, focal adhesions formed in DPSC (24 h post-seeding)

were qualitatively and quantitatively evaluated (Fig. 3.12 A and C). Obtained results indicated that compared to pure PLA samples, the PLA+ECM surface ($p < 0.001$) resulted a higher number of focal adhesions within the cells, i.e. ECM coated scaffolds were more attractive for DPSC attachment.

All in all, results revealed that cell derived ECM proteins significantly improve DPSC adhesion.

3.3.2 Impact of cell-derived ECM coated scaffolds on cell migration and proliferation

To determine whether ECM proteins stimulate and initiate cellular motility and proliferation, DPSC migration and proliferation assays were performed.

For cell migration testing, scaffolds were incubated on a monolayer of DPSCs for 72 h, and then the number of cells that have migrated onto these specimens was determined (Fig. 3.13 A). Obtained results showed that for DPSCs migration, ECM coated surface was more attractive. Compared to pure PLA samples, higher cell count was determined on PLA+ECM scaffolds ($p < 0.05$).

The assessment of cell proliferation activity (Fig. 3.13 B) indicated that, cell numbers registered 24, 48 and 72 h post-seeding were almost the same on both scaffolds (PLA and PLA+ECM), i.e., DPSC proliferated equally well on both groups of specimens. However, differences between PLA and PLA+ECM groups appeared 96 and 120 h post-seeding. During these time intervals, DPSCs showed significantly better proliferative activity on PLA+ECM scaffolds compared to PLA ones

Obtained results of DPSC migration and proliferation showed that ECM proteins had a positive impact on both cell migration and proliferation.

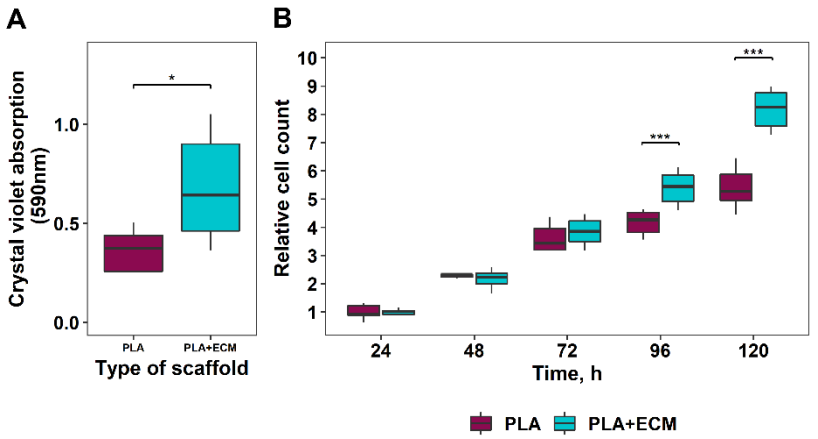

Figure 3.13. DPSC migration and proliferation on ECM coated scaffolds. A – evaluation of vertical cell migration onto the scaffolds using crystal violet assay; B – relative DPSC proliferation rate; data is standardized according to the number of cells maintained on appropriate scaffolds for 24 h. Results are presented as median ± IQR. Statistically significant results indicated as * ($p<0.05$) and *** ($p<0.001$).

In conclusion, it can be stated that DPSC-derived ECM initiated enhanced cell adhesion, migration, and proliferation. Natural tissue ECM is composed of dense network of various proteins (collagens, fibronectin, vitronectin, etc.) and proteoglycans (versican, decorin, biglycan etc.) that provide the environment which is required for tissue cell vitality (Kim et al., 2018). Similar ECM network can also be synthesised by *in vitro* cell culture (Thibault et al., 2011). Therefore, MSCs seeded on decellularized surfaces, via integrin receptors interact with the amino acid sequences presented in ECM proteins and proteoglycans. Respectively, proteins involved in cell adhesion (e.g., vinculin) and cytoskeleton formation (e.g., actin) processes will be attracted to these interaction sites (Kumar et al., 2016; Humphries et al., 2007). These proteins further activate signalling pathways involved in MSC survival, proliferation or

differentiation (Holle et al., 2016; Kumar et al., 2016; Provenzano and Keely, 2011).

3.3.3 Influence of cell-derived ECM coated scaffolds on cell osteogenesis

To determine the cell-derived ECM effect on the induction of DPSC osteogenic differentiation, ALP activity, osteogenic-related gene expression and bone tissue specific ECM were analysed. The obtained results will be discussed sequentially, according to the order of osteogenesis process in the organism (Burr and Allen, 2014).

Runx2 and OPN proteins gene expression analysis results showed that both tested scaffolds stimulated DPSC differentiation towards osteogenic lineage by upregulation of Runx2 and OPN gene expression (Fig. 3.14). Moreover, the highest Runx2 protein gene expression was determined in cells maintained on both tested scaffolds at 10^{th} day of differentiation (Fig. 3.14). However, already after 1st day of differentiation in DPSCs grown on PLA+ECM, gene expression level of this protein showed greater increase compared to cells grown on pure PLA ($p<0.05$). In the case of OPN protein gene expression, it remained almost unchanged at 1^{st} and 7^{th} differentiation evaluation days (Fig. 3.14), whereas the highest level of expression was observed only at 10th day of differentiation in cells grown on both investigated scaffolds. However, statistically significant difference of OPN protein gene expression induction in DPSCs cultivated on PLA and PLA+ECM scaffolds was not detected.

Results of ALP activity indicated (Fig. 3.15 A) that after 1st and 7th differentiation days PLA and PLA+ECM scaffolds did not cause differences in the activity of this protein within the cells. The highest ALP activity, in the cells maintained on PLA and PLA+ECM scaffolds, was detected after 10 days of differentiation. However,

stronger ALP activity was registered in DPSCs grown on ECM coated scaffolds ($p < 0.05$) compared to pure PLA samples.

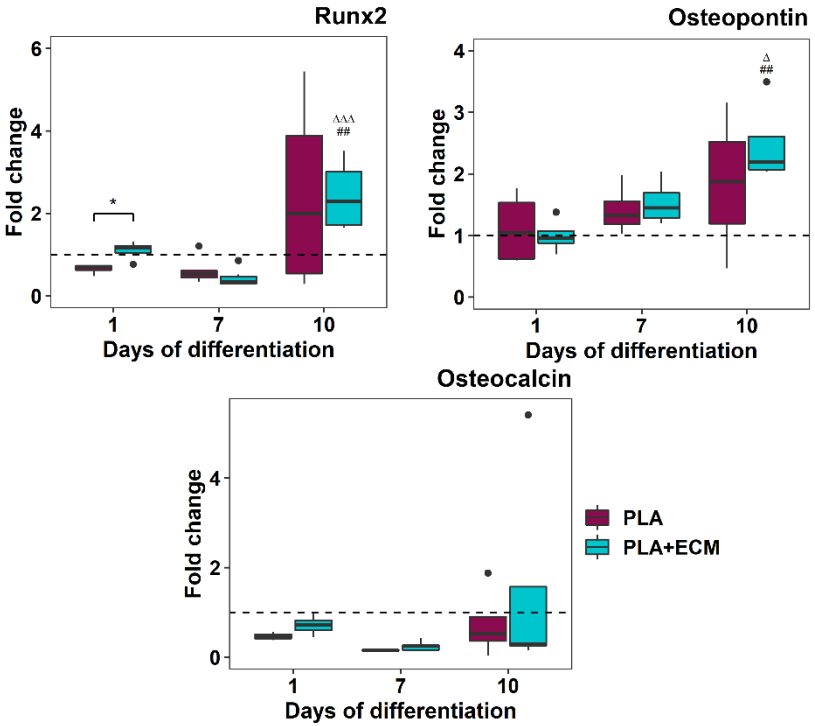

Figure 3.14 Osteogenesis-related proteins (Runx2, OPN, OCN) genes expression levels in DPSC grown on cell-derived ECM coated scaffolds. Results are presented as median ± IQR. Statistically significant differences between cells grown on different scaffolds groups are marked with * ($p<0.05$), while # shows statistically significant differences compared to day 1 within the same scaffold group – ## ($p<0.01$), Δ demonstrates a significant differences compared to day 7 within the same scaffold group – Δ ($p<0.05$), ΔΔΔ ($p<0.001$).

Bone tissue-specific ECM formation results showed, that DPSCs grown on both surfaces tended to accumulate collagen in their ECM, however, significant differences between PLA and PLA+ECM scaffolds impact on collagen accumulation were not observed (Fig. 3.15 B). In contrast, ECM mineralisation results indicated that after 7 and 10 days of DPSC cultivation on scaffolds, the greatest and statistically significant increase of ECM mineralisation was registered in cell cultures maintained on PLA+ECM specimens compared to pure PLA samples (respectively – 7^{th} day $p<0.001$, 1^{st} day $p<0.05$) (Fig. 3.15 C).

Differences in OCN protein gene expression were not observed at any time point in cells grown on both tested scaffold groups (Fig. 3.14). Most likely, as in case of substrate topography and composite scaffolds experiments, DPSCs did not have enough time to reach the late stage of osteogenic differentiation, to completely differentiate into osteoblasts (Huang et al., 2007).

Obtained results indicated that both scaffolds groups (PLA and PLA+ECM) initiated spontaneous DPSC osteogenic differentiation. However, PLA+ECM scaffolds demonstrated stronger osteoinductive properties. Better PLA+ECM osteoinductivity can be explained by DPSC derived ECM. Decellularized surfaces were rich in calcium deposits, which serves as nucleation sites for new HA crystal formation (Liao et al., 2010b). As a consequence, in order to form new HA crystals in ECM, cells have to enhance ALP phosphatase activity (Mitton-Fitzgerald et al., 2016; Rosen, 2013; Orimo, 2010). Therefore, higher ECM mineralisation and ALP activity were observed in DPSCs grown on PLA+ECM scaffolds.

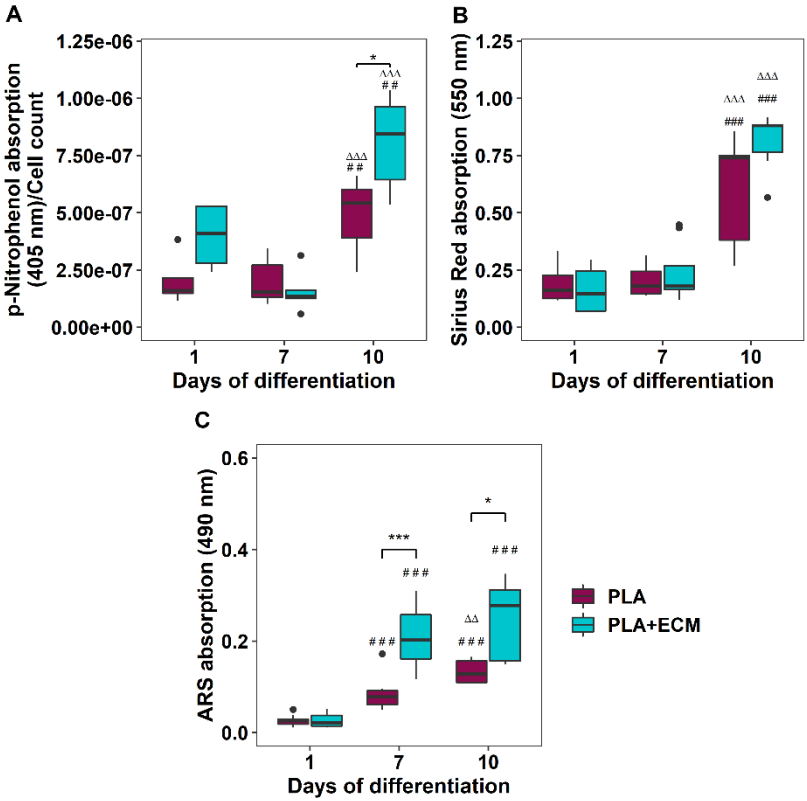

Figure 3.15. Osteogenic differentiation assessment. A – ALP activity evaluated by p-nitrophenol assay; B – DPSCs collagen production evaluated by Sirius Red staining; C – ECM mineralization analysis by ARS staining. Results are presented as median ± IQR. Statistically significant differences between different scaffolds groups are marked with * ($p<0.05$) and *** ($p<0.001$), while # shows statistically significant differences compared to day 1 within the same scaffold group – ### ($p<0.001$), Δ demonstrates significant differences compared to day 7 within the same scaffold group – ΔΔ ($p<0.01$).

3.4 Potential response of organism to different artificial bone tissue constructs

One of the strategies used to regenerate diseased tissues are stem cell-scaffold constructs. Such *in vitro*-created construct of stem cells and scaffold is not a fully functional artificial tissue yet. However, studies have shown that it can still provide efficient regeneration of damaged tissue areas (Diomede et al., 2016; El-Backly et al., 2008). It was observed that even after a detailed analysis of scaffold and stem cells interaction *in vitro*, the construct still produces inflammation after implantation to organism (Lock et al., 2019). Therefore, in this work, using different *in vitro* assays we tried to evaluate a potential response of patient's organism to different (DPSC-PLA, DPSC-PLA+HA, DPSC-PLA+BG, and DPSC-PLA+ECM) artificial bone constructs.

3.4.1 Construct (DPSC-scaffold) signal to the organism

To determine whether scaffold chemical composition and its surface decoration with ECM initiate different cell signalling, DPSCs were grown on different scaffolds (PLA, PLA+HA, PLA+BG, PLA+ECM) and their expressed cytokines, chemokines, and growth factors were analysed.

The signalling molecule analysis was performed after 7 days of DPSC cultivation on tested scaffolds. The 7-day interval was chosen according to previous results, which showed that after 7 days of DPSC cultivation on scaffolds the osteogenesis process was already active. Therefore, after implantation to the organism, the 7 days construct would interact with recipient tissue cells, thereby stimulating new bone tissue formation in the damaged area.

The expression of 29 molecules was analysed by Dot Blot (Fig. S4), 11 of which were detected. In secretomes collected from all four constructs (DPSC-PLA, DPSC-PLA+HA, DPSC-PLA+BG and DPSC-PLA+ECM) the expression of the following cytokines, chemokines and growth factors was observed: cytokine-inducible neutrophil chemoattractant family proteins (CINC) (CINC-1, CINC-2α / β, CINC-3), chemokine (CXC motif) ligand 1 (CXCL1), interleukin 1ra (IL-1ra), interleukin 6 (IL-6), soluble intercellular adhesion molecule 1 (sICAM-1), CXC motif chemokine 1 (CXCL10), chemokine (CC motif) ligand 5 (CCL5), TIMP metallopeptidase inhibitor 1 (TIMP-1), and VEGF (Fig. 3.16). However, significant differences between constructs` impact on the amount of detected signalling molecules were not observed. Usually, most of the determined molecules are associated with activation (e.g., IL-6, CINC family proteins, etc.) or inhibition (e.g., interleukin 10, interleukin 13, etc.) of inflammatory processes (Su et al., 2012; Cavaillon, 2001). Still, depending on the cell type which synthesizes them, they may initiate processes unrelated with the immune response. For example, studies have shown that pro-inflammatory cytokines, IL-6 and CINC family proteins, can activate osteogenic differentiation signalling pathways in MSCs (Huang et al., 2018b; Xie et al., 2018; Yang et al., 2018; Chung et al., 2006). Such osteogenesis-inducing effect was demonstrated by other molecules which were found in secretomes (Liu et al., 2014; Egea et al., 2012; Koizumi et al., 2009; Xiao et al., 2009; Fernandes et al., 2008; Lisignoli et al., 2003). Therefore, it can be stated, that according to *in vitro* results, all tested constructs after implantation would initiate bone tissue regeneration without causing inflammation.

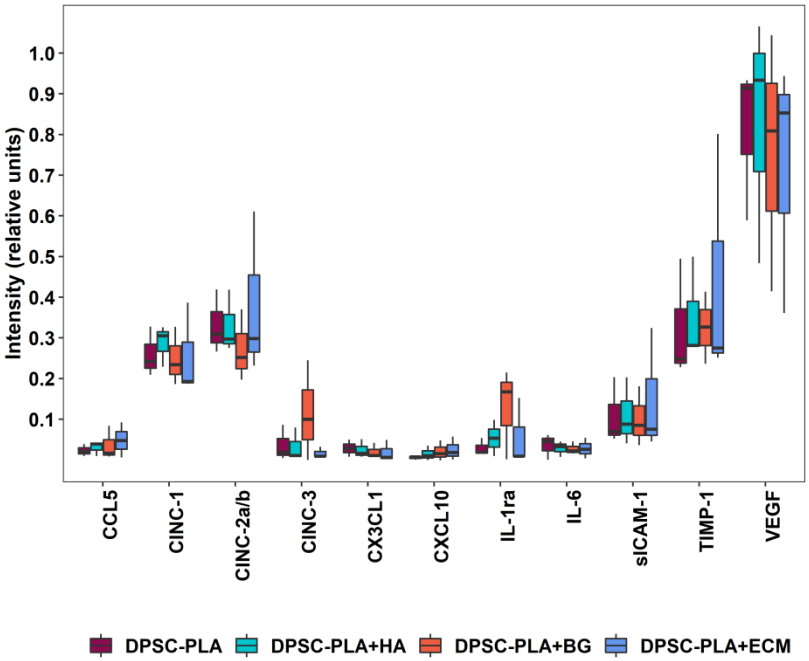

Figure 3.16. Cytokines, chemokines and growth factors detected in secretomes of DPSC-PLA, DPSC-PLA+HA, DPSC-PLA+BG or DPSC-PLA+ECM constructs. Signalling molecules were analysed by Dot Blot. Data were normalized according to the mean values of positive control. Results are presented as median ± IQR.

Moreover, it was noticed that DPSCs, which grew on all four tested scaffolds (PLA, PLA+HA, PLA+BG, or PLA+ECM) most actively synthesized the growth factor VEGF. Identified amount of VEGF in secretomes was highest compared to other molecules (Fig. 3.16). This factor is closely associated with the induction of angiogenesis (McColl et al., 2004), thus it can be stated that all investigated constructs after implantation would initiate vascular network formation in newly formed bone.

3.4.2 Construct (DPSC-scaffold) impact on induction of angiogenesis

Artificial construct will not ensure successful tissue regeneration unless a new vascular network is formed in and around damaged tissue area. For this reason, constructs should not only exhibit excellent biocompatibility, as well as, stimulation of stem cell differentiation, but they also should initiate the angiogenesis process (Chen et al., 2018a; Krishnan et al., 2014). Therefore, the angioinductive properties of different artificial bone tissue constructs (DPSC-PLA, DPSC-PLA+HA, DPSC-PLA+BG or DPSC-PLA+ECM) were analysed in this work. Transfected cell culture (red fluorescent PKEL-R) was created and used for angiogenesis analysis.

In order to ensure endothelial cells migration to the damaged tissue area, it is important that the construct would initiate this process. Therefore, scaffolds alone (PLA, PLA+HA, PLA+BG, PLA+ECM) and their combinations with DPSCs (constructs) impact on PKEL migration was analysed.

To assess PKEL migration on the scaffolds, a quantitative, vertical migration test was performed. Scaffolds were incubated on a monolayer of PKELs for 72 h, and then the number of cells migrated onto these specimens was determined (Fig. 3.17 A). Results showed that the most attractive for PKELs were PLA+BG and PLA+ECM samples. These types of scaffolds initiated the best cell migration compared to pure PLA (PLA:PLA+BG – $p<0.01$, and PLA:PLA+ECM – $p<0.001$) and composite PLA+HA (PLA:PLA+BG – $p<0.05$, and PLA:PLA+ECM – $p<0.01$) specimens.

PKEL migration on constructs (DPSC-PLA, DPSC-PLA+HA, DPSC-PLA+BG and DPSC-PLA+ECM) was evaluated qualitatively. Constructs were incubated on a monolayer of PKEL-Rs for 3 and 72 h, and then the cells migrated onto the specimens was visualized

using fluorescence microscope. It was observed that within the first 3 hours cell migration did not occur on any construct type (Fig. 3.17 B). However, after 72 hours, vessel-like structures formed by PKEL-R were observed on all tested specimens.

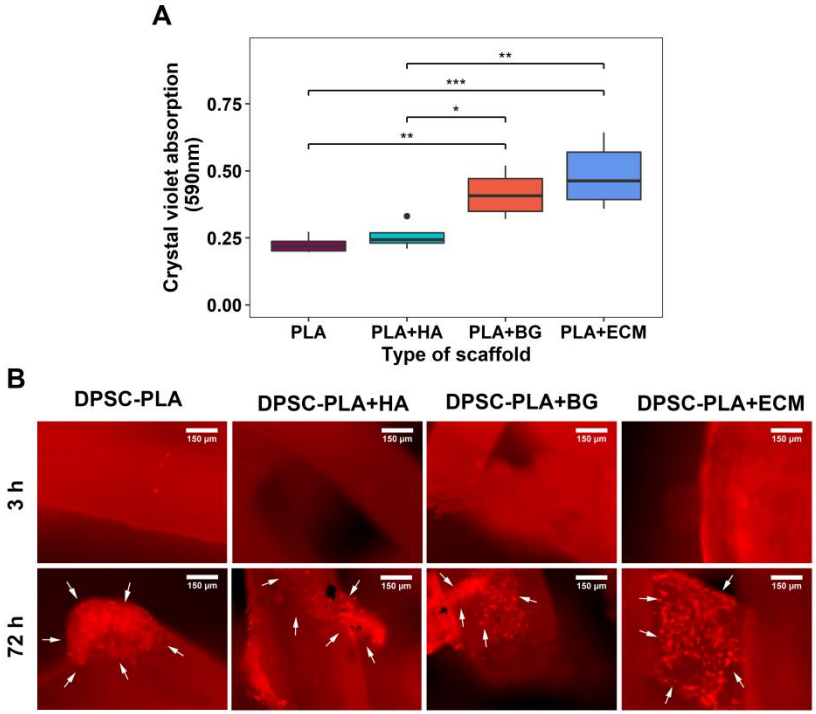

Fig 3.17. Evaluation of PKEL migration on scaffolds and constructs. A - quantitative evaluation of PKEL migration on PLA, PLA+HA, PLA+BG, and PLA+ECM scaffolds using crystal violet assay. Results are presented as median ± IQR. Statistically significant differences between different scaffolds groups were marked as "*" when $p < 0.05$, "**" when $p < 0.01$, and "***" when $p < 0.001$; B – qualitative assessment of PKEL migration on constructs (DPSC-scaffold). Red colour, PKEL (PKEL-R) transfected with lentiviral vector pLJM1-mCherry; blue colour, DAPI staining.

The assessment of PKEL migration on scaffolds and constructs confirmed the hypothesis that tested samples demonstrate angioinductive properties. We believe that the best cell migration onto PLA+BG and PLA+ECM samples was determined by the scaffold chemical composition or surface coating with ECM, respectively. In the case of PLA+BG scaffolds, such improved PKEL migration was initiated by 45S5 BG particles. Studies have shown that during BG degradation, various ions are released into growth medium, which stimulate cell migration and angiogenesis (Li et al., 2016; Yu et al., 2016; Day, 2005). For PLA+ECM scaffolds, PKEL migration was mediated by the DPSC-derived ECM network which covered the scaffold surface. Proteins presented in ECM are capable to initiate cell migration and angiogenesis (Noh et al., 2016; Moore et al., 2015; Pati et al., 2015; Cheng et al., 2014; Chen, 2010). Whereas, after construct implantation into the body, the vascular network formation is stimulated by both - construct forming scaffold and cells (Liu et al., 2011), thus DPSC-PLA+BG and DPSC-PLA+ECM constructs should initiate the most effective angiogenesis in the organism.

Results application for artificial bone tissue development

Analysis of substrate macrophotography (>100 μm) impact on the fate of DPSCs revealed that for spontaneous cell osteogenesis induction the precise structuring of the scaffold (nano- and micro-surface patterns) is not necessarily required. To induce spontaneous DPSCs osteogenic differentiation, it is sufficient enough to produce FFF-derived, 3D printed, interconnected porosity scaffold, in which each layer is formed of two threads moulded together. After evaluating the impact of surface chemical composition on cell behavior, it was observed that stem cell osteogenesis is stimulated

most efficiently by PLA and BG composite. Moreover, it was demonstrated that PLA surface coating with DPSC-derived ECM network significantly improves the osteoinductive properties of the surface. The *in vitro* assay of constructs (made of scaffolds (PLA, PLA+HA, PLA+BG and PLA+ECM) and DPSCs) ability to initiate angiogenesis revealed that DPSC-PLA+BG and DPSC-PLA+ECM constructs would be most suitable for this process induction in the organism. Therefore, we think that by combining DPSCs, composite PLA+BG macrostructured scaffold and DPSC-derived ECM network it can be expected to reach successful bone tissue regeneration *in vivo*. The results of this work significantly contribute to successful artificial bone construction, which would lead to a breakthrough in modern medicine.

CONCLUSIONS

1. It was shown that surface macrotopography (>100 μm) alters the morphology of dental pulp stem cells (DPSC); shape change-induced cytoskeletal tension initiate proliferation and spontaneous osteogenic differentiation of these cells.
2. It was determined that composite of polylactic acid and 10% 45S5 Bioglass (PLA+BG) was more attractive for DPSC migration compared to PLA and 10% hydroxyapatite (PLA+HA) surface, but PLA+HA substrate was more suitable for cell attachment and proliferation.
3. Results showed that both types of investigated composite scaffolds initiated osteogenesis processes in the cells, however, PLA+BG composite promoted the earliest and the strongest alkaline phosphatase activity, extracellular matrix mineralization and osteogenic-related proteins Runx2 and OPN genes expression levels.
4. It was demonstrated that PLA scaffold surface coating with extracellular matrix (ECM) proteins improves DPSC attachment, moreover, compared to uncoated polymer, this substrate is more attractive for cell migration and proliferation.
5. It was determined that cell-derived ECM protein network increases the osteoinductivity of the polymer scaffold; as cells grow on such substrate, higher alkaline phosphatase activity and ECM mineralization was observed.
6. Only cytokines, chemokines, and growth factors (CINC-1, CINC-2α / β, CINC- 3, CXCL1, IL-1ra, IL-6, sICAM-1, CXCL10, CCL5, TIMP-1 and VEGF), promoting osteoregenerative process, were secreted by cells on all examined composites (DPSC-PLA, DPSC-PLA+HA, DPSC-PLA+BG and DPSC-PLA+ECM); pro-inflammatory molecules have not been identified. Evaluation of construct-initiated angiogenesis showed that this process was most intensely induced by DPSC-PLA+BG and DPSC-PLA+ECM samples. Obtained results suggest that DPSC-PLA+BG and DPSC-PLA+ECM constructs are most suitable for bone regeneration in the organism.

SUMMARY IN LITHUANIAN

Temos aktualumas

Kasmet milijonai žmonių visame pasaulyje, dėl genetinių ligų, vėžinių susirgimų, kaulo rezorbcijų ar infekcijų, patiria kaulinio audinio pažeidimus kurie patys savaime regeneruoti nebegali. Tokie pažeidimai klinikoje yra gydomi naudojant kaulinio audinio transplantatus arba tam tikras sintetines medžiagas. Tačiau pastarosios dar negeba pilnai atkurti ir prisitaikyti prie specifinių kaulinio audinio funkcijų, o naudojami transplantatai paciento organizmo yra dažnai atmetami. Todėl siekiama sukurti dirbtinius kaulinio audinio konstruktus, kurie eliminuotų dabar medicinoje naudojamų technologijų trūkumus, būtų personalizuoti bei santykinai nebrangiai pagaminami. Nors šioje srityje jau pasiekta daug, tačiau vis dar nėra iki galo priimta kokios paviršiaus geometrijos yra tinkamiausios tokio konstrukto gamybai, neapsisprendžiama kokias medžiagas ir gamybos būdą tam reikėtų naudoti, bei kokias ląsteles ir bioaktyvias molekulias pasirinkti.

Darbo tikslas ir uždaviniai

Tikslas: nustatyti skirtingų substrato modifikacijų įtaką kamieninių ląstelių likimui siekiant sukonstruoti funkcionalų dirbtinį kaulinį audinį.

Uždaviniai:
1. Ištirti paviršiaus makrotopografijos (>100 μm) vaidmenį dantų pulpos kamieninių ląstelių (DPSC) likimui.
2. Įvertinti substrato cheminės sudėties įtaką DPSC gyvybiniams procesams.

3. Atlikti medžiagos cheminės sudėties vaidmens ląstelių osteogenezei analizę.
4. Nustatyti substrato biodekoravimo poveikį DPSC judrumui, prisitvirtinimui bei dauginimuisi.
5. Įvertinti paviršiaus dekoravimo įtaką ląstelių diferenciacijai osteogenine kryptimi.
6. In vitro sąlygomis modeliuoti ir įvertinti ląstelių-karkaso konstrukto siunčiamą signalą recipientiniams audiniams.

Pagrindiniai darbo rezultatai ir mokslinis naujumas

Iki šiol buvo žinoma, kad tik nano- ir mikro- paviršiaus topografijos gali reguliuoti ląstelės lemtį. Šiame darbe pademonstruota, kad ir FFF 3D spausdinimo metodu pagamintų makro- paviršiaus topografijų (>100 μm) pilnai pakanka tam jog substratas inicijuotų spontainius osteogenezės procesus ląstelėse. Tai rodo, kad FFF 3D spausdinimas gali būti sėkmingai taikomas pigiai, našiai ir personalizuotai konstruktų skirtų kaulinio audinio regeneracijai gamybai.

Darbe pirmą kartą palygintos iš PLA+HA ir PLA+BG kompozitų FFF 3D spausdinimo būdu pagamintų karkasų biofizikinės bei osteo- ir angio- indukcinės savybės. Nustatyta, kad PLA+BG kompozitas *in vitro* sąlygomis yra tinkamesnis dirbtinio kaulinio audinio konstravimui. Šie rezultatai naudingi dirbtinių kaulinio audinio konstruktų gamybos optimizacijai.

Taipogi, darbe tirta daug žadanti karkasų dekoravimo technologija – paviršiaus padengimas ląstelių kilmės TU. Čia ji pirmą kartą taikyta naudojant pirmines DPSC bei FFF 3D spausdinimo metodu pagamintą PLA karkasą. Pastebėta, kad DPSC suformuotas TU pastebimai pagerina konstrukto osteo- ir angioinduktyvumą *in vitro*.

Todėl manome, kad tarpusavyje apjungus DPSC ląsteles, kompozitinį PLA+BG porėtos makrostruktūros karkasą bei DPSC

susintetintą TU tinklą galima tikėtis pasiekti sėkmingos kaulinio audinio regeneracijos *in vivo*.

Šis mokslinis darbas svariai prisideda prie audinių inžinerijos progreso kuriant dirbtinį kaulinį audinį, kuris taptu proveržiu šiuolaikinėje medicinoje.

REFERENCES

1. Abagnale G, Sechi A, Steger M, Zhou Q, Kuo C-C, Aydin G, Schalla C, Müller-Newen G, Zenke M, Costa IG, van Rijn P, Gillner A, Wagner W. Surface Topography Guides Morphology and Spatial Patterning of Induced Pluripotent Stem Cell Colonies. *Stem Cell Reports*. 2017;9:654–66. PMid:28757164. doi: https://doi.org/10.1016/j.stemcr.2017.06.016.
2. Abagnale G, Steger M, Nguyen VH, Hersch N, Sechi A, Joussen S, Denecke B, Merkel R, Hoffmann B, Dreser A, Schnakenberg U, Gillner A, Wagner W. Surface topography enhances differentiation of mesenchymal stem cells towards osteogenic and adipogenic lineages. *Biomaterials*. 2015;61:316–26. PMid:26026844. doi: https://doi.org/10.1016/j.biomaterials.2015.05.030.
3. Alksne M, Simoliunas E, Kalvaityte M, Skliutas E, Rinkunaite I, Gendviliene I, Baltriukiene D, Rutkunas V, Bukelskiene V. The effect of larger than cell diameter polylactic acid surface patterns on osteogenic differentiation of rat dental pulp stem cells. *J Biomed Mater Res - Part A*. 2019;107. doi: https://doi.org/10.1002/jbm.a.36547.
4. Anselme K. Osteoblast adhesion on biomaterials. *Biomaterials*. 2000;21:667–81. PMid:10711964. .
5. Di Benedetto A, Brunetti G, Posa F, Ballini A, Grassi FR, Colaianni G, Colucci S, Rossi E, Cavalcanti-Adam EA, Lo Muzio L, Grano M, Mori G. Osteogenic differentiation of mesenchymal stem cells from dental bud: Role of integrins and cadherins. *Stem Cell Res*. 2015;15:618–28. doi: https://doi.org/10.1016/j.scr.2015.09.011.
6. Bhat S, Kumar A. Cell proliferation on three-dimensional chitosan–agarose–gelatin cryogel scaffolds for tissue engineering applications. *J Biosci Bioeng*. 2012;114:663–70. PMid:22884715. doi: https://doi.org/10.1016/j.jbiosc.2012.07.005.
7. Burgio F, Rimmer N, Pieles U, Buschmann J, Beaufils-Hugot M. Characterization and in ovo vascularization of a 3D-printed

hydroxyapatite scaffold with different extracellular matrix coatings under perfusion culture. *Biol Open*. 2018;7:bio034488. PMid:30341104. doi: https://doi.org/10.1242/bio.034488.
8. Burr DB, Allen MR. Basic and Applied Bone Biology. Elsevier; 2014. doi: https://doi.org/10.1016/C2011-0-05817-9.
9. Castells-Sala Cristina, Alemany-Ribes Mireia et al. Current Applications of Tissue Engineering in Biomedicine. *J Biochips Tissue Chips*. 2015;s2:1–14. doi: https://doi.org/10.4172/2153-0777.S2-004.
10. Cavaillon JM. Pro- versus anti-inflammatory cytokines: myth or reality. *Cell Mol Biol (Noisy-Le-Grand)*. 2001;47:695–702. PMid:11502077. .
11. Chaubey A, Ross KJ, Leadbetter RM, Burg KJL. Surface Patterning: Tool to Modulate Stem Cell Differentiation in an Adipose System. *J Biomed Mater Res Part B Appl Biomater*. 2008;84:70–8. doi: https://doi.org/10.1002/jbm.b.30846.
12. Chen J, Deng L, Porter C, Alexander G, Patel D, Vines J, Zhang X, Chasteen-Boyd D, Sung H-J, Li Y-P, Javed A, Gilbert S, Cheon K, Jun H-W. Angiogenic and Osteogenic Synergy of Human Mesenchymal Stem Cells and Human Umbilical Vein Endothelial Cells Cocultured on a Nanomatrix. *Sci Rep*. 2018a;8:15749. PMid:30356078. doi: https://doi.org/10.1038/s41598-018-34033-2.
13. Chen Q, Cao L, Wang J-L, Zhao H, Lin H, Fan Z-Y, Dong J. Improved cell adhesion and osteogenesis using a PLTGA (poly l -lactide, 1,3-trimethylene carbonate, and glycolide) terpolymer by gelatin-assisted hydroxyapatite immobilization for bone regeneration. *J Mater Chem B*. 2018b;6:301–11. doi: https://doi.org/10.1039/C7TB02293J.
14. Chen XD. Extracellular matrix provides an optimal niche for the maintenance and propagation of mesenchymal stem cells. *Birth Defects Res Part C - Embryo Today Rev*. 2010;90:45–54. doi: https://doi.org/10.1002/bdrc.20171.
15. Cheng CW, Solorio LD, Alsberg E. Decellularized tissue and cell-derived extracellular matrices as scaffolds for orthopaedic tissue engineering. *Biotechnol Adv*. 2014;32:462–84. doi: https://doi.org/10.1016/j.biotechadv.2013.12.012.
16. Chung R, Cool JC, Scherer MA, Foster BK, Xian CJ. Roles of

neutrophil-mediated inflammatory response in the bony repair of injured growth plate cartilage in young rats. *J Leukoc Biol*. 2006;80:1272–80. doi: https://doi.org/10.1189/jlb.0606365.
17. Cooper GM. Cell Proliferation in Development and Differentiation. 2000.
18. Day RM. Bioactive glass stimulates the secretion of angiogenic growth factors and angiogenesis in vitro. *Tissue Eng*. 2005;11:768–77. doi: https://doi.org/10.1089/ten.2005.11.768.
19. Deligianni DD, Katsala ND, Koutsoukos PG, Missirlis YF. Effect of surface roughness of hydroxyapatite on human bone marrow cell adhesion, proliferation, differentiation and detachment strength. *Biomaterials*. 2001;22:87–96. PMid:11085388. .
20. DiMilla PA, Barbee K, Lauffenburger DA. Mathematical model for the effects of adhesion and mechanics on cell migration speed. *Biophys J*. 1991;60:15–37. doi: https://doi.org/10.1016/S0006-3495(91)82027-6.
21. Diomede F, Zini N, Gatta V, Fulle S, Merciaro I, D'Aurora M, La Rovere RM, Traini T, Pizzicannella J, Ballerini P, Caputi S, Piattelli A, Trubiani O. Human periodontal ligament stem cells cultured onto cortico-cancellous scaffold drive bone regenerative process. *Eur Cell Mater*. 2016;32:181–201. PMid:27633707. doi: https://doi.org/10.22203/ecm.v032a12.
22. Du Y, Montoya C, Orrego S, Wei X, Ling J, Lelkes PI, Yang M. Topographic cues of a novel bilayered scaffold modulate dental pulp stem cells differentiation by regulating YAP signalling through cytoskeleton adjustments. *Cell Prolif*. 2019. doi: https://doi.org/10.1111/cpr.12676.
23. Egea V, Zahler S, Rieth N, Neth P, Popp T, Kehe K, Jochum M, Ries C. Tissue inhibitor of metalloproteinase-1 (TIMP-1) regulates mesenchymal stem cells through let-7f microRNA and Wnt/β-catenin signaling. *Proc Natl Acad Sci U S A*. 2012;109. doi: https://doi.org/10.1073/pnas.1115083109.
24. El-Backly RM, Massoud AG, Azza ;, El-Badry M, Sherif RA, Marei MK. Regeneration of dentine/pulp-like tissue using a dental pulp stem cell/poly(lactic-co-glycolic) acid scaffold construct in New Zealand white rabbits. 2008. doi: https://doi.org/10.1111/j.1747-4477.2008.00139.x.

25. Fernandes JC, Shi Q, Benderdour M, Lajeunesse D, Lavigne P. An active role for soluble and membrane intercellular adhesion molecule-1 in osteoclast activity in vitro. *J Bone Miner Metab*. 2008;26:543–50. doi: https://doi.org/10.1007/s00774-008-0866-0.
26. Gorbunoff MJ, Timasheff SN. The interaction of proteins with hydroxyapatite: III. Mechanism. *Anal Biochem*. 1984;136:440–5. doi: https://doi.org/10.1016/0003-2697(84)90241-0.
27. Hamilton D, Ghrebi S, Kim H, Chehroudi B, Brunette D. Surface Topography and Cell Behavior. Encycl. Biomater. Biomed. Eng. Second Ed. - Four Vol. Set, CRC Press; 2008, p. 2551–61. doi: https://doi.org/10.1201/b18990-246.
28. Hannink G, Arts JJC. Bioresorbability, porosity and mechanical strength of bone substitutes: What is optimal for bone regeneration? *Injury*. 2011;42:S22–5. PMid:21714966. doi: https://doi.org/10.1016/j.injury.2011.06.008.
29. Holle AW, McIntyre AJ, Kehe J, Wijesekara P, Young JL, Vincent LG, Engler AJ. High content image analysis of focal adhesion-dependent mechanosensitive stem cell differentiation. *Integr Biol (United Kingdom)*. 2016;8:1049–58. doi: https://doi.org/10.1039/c6ib00076b.
30. Howard D, Buttery LD, Shakesheff KM, Roberts SJ. Tissue engineering: strategies, stem cells and scaffolds. *J Anat*. 2008;213:66–72. PMid:18422523. doi: https://doi.org/10.1111/j.1469-7580.2008.00878.x.
31. Huang B, Caetano G, Vyas C, Blaker JJ, Diver C, Bártolo P. Polymer-Ceramic Composite Scaffolds: The Effect of Hydroxyapatite and β-tri-Calcium Phosphate. *Mater (Basel, Switzerland)*. 2018a;11. PMid:29342890. doi: https://doi.org/10.3390/ma11010129.
32. Huang RL, Sun Y, Ho CK, Liu K, Tang QQ, Xie Y, Li Q. IL-6 potentiates BMP-2-induced osteogenesis and adipogenesis via two different BMPR1A-mediated pathways article. *Cell Death Dis*. 2018b;9. doi: https://doi.org/10.1038/s41419-017-0126-0.
33. Huang W, Yang S, Shao J, Li Y-P. Signaling and transcriptional regulation in osteoblast commitment and differentiation. *Front Biosci*. 2007;12:3068–92. PMid:17485283. .
34. Humphries JD, Wang P, Streuli C, Geiger B, Humphries MJ,

Ballestrem C. Vinculin controls focal adhesion formation by direct interactions with talin and actin. *J Cell Biol*. 2007;179:1043–57. doi: https://doi.org/10.1083/jcb.200703036.
35. Huttenlocher A, Sandborg RR, Horwitz AF. Adhesion in cell migration. *Curr Opin Cell Biol*. 1995;7:697–706. doi: https://doi.org/10.1016/0955-0674(95)80112-X.
36. Janners MY, Searls RL. Changes in rate of cellular proliferation during the differentiation of cartilage and muscle in the mesenchyme of the embryonic chick wing. *Dev Biol*. 1970;23:136–65. doi: https://doi.org/10.1016/S0012-1606(70)80011-2.
37. Kajita M, Hogan C, Harris AR, Dupre-Crochet S, Itasaki N, Kawakami K, Charras G, Tada M, Fujita Y. Interaction with surrounding normal epithelial cells influences signalling pathways and behaviour of Src-transformed cells. *J Cell Sci*. 2010;123:171–80. PMid:20026643. doi: https://doi.org/10.1242/jcs.057976.
38. Karageorgiou V, Kaplan D. Porosity of 3D biomaterial scaffolds and osteogenesis. *Biomaterials*. 2005;26:5474–91. PMid:15860204. doi: https://doi.org/10.1016/j.biomaterials.2005.02.002.
39. Kilian KA, Bugarija B, Lahn BT, Mrksich M, Kiessling LL. Geometric cues for directing the differentiation of mesenchymal stem cells. *PNAS*. 2010;107:4872–7. doi: https://doi.org/10.1073/pnas.0903269107.
40. Kim B, Ventura R, Lee B-T. Functionalization of porous BCP scaffold by generating cell-derived extracellular matrix from rat bone marrow stem cells culture for bone tissue engineering. *J Tissue Eng Regen Med*. 2018;12:e1256–67. doi: https://doi.org/10.1002/term.2529.
41. Kim J-W, Shin K-H, Koh Y-H, Hah MJ, Moon J, Kim H-E. Production of Poly(ε-Caprolactone)/Hydroxyapatite Composite Scaffolds with a Tailored Macro/Micro-Porous Structure, High Mechanical Properties, and Excellent Bioactivity. *Mater (Basel, Switzerland)*. 2017;10. PMid:28937605. doi: https://doi.org/10.3390/ma10101123.
42. Kim SE, Yun Y-P, Shim K-S, Kim H-J, Park K, Song H-R. 3D printed alendronate-releasing poly(caprolactone) porous

scaffolds enhance osteogenic differentiation and bone formation in rat tibial defects. *Biomed Mater*. 2016;11:055005. doi: https://doi.org/10.1088/1748-6041/11/5/055005.
43. Kim YS, Majid M, Melchiorri AJ, Mikos AG. Applications of decellularized extracellular matrix in bone and cartilage tissue engineering. *Bioeng Transl Med*. 2019;4:83–95. doi: https://doi.org/10.1002/btm2.10110.
44. Klammert U, Gbureck U, Vorndran E, Rödiger J, Meyer-Marcotty P, Kübler AC. 3D powder printed calcium phosphate implants for reconstruction of cranial and maxillofacial defects. *J Cranio-Maxillofacial Surg*. 2010;38:565–70. doi: https://doi.org/10.1016/J.JCMS.2010.01.009.
45. Koizumi K, Saitoh Y, Minami T, Takeno N, Tsuneyama K, Miyahara T, Nakayama T, Sakurai H, Takano Y, Nishimura M, Imai T, Yoshie O, Saiki I. Role of CX3CL1/Fractalkine in Osteoclast Differentiation and Bone Resorption. *J Immunol*. 2009;183:7825–31. doi: https://doi.org/10.4049/jimmunol.0803627.
46. Krishna L, Dhamodaran K, Jayadev C, Chatterjee K, Shetty R, Khora SS, Das D. Nanostructured scaffold as a determinant of stem cell fate. *Stem Cell Res Ther*. 2016;7. doi: https://doi.org/10.1186/s13287-016-0440-y.
47. Krishnan L, Willett NJ, Guldberg RE. Vascularization Strategies for Bone Regeneration. *Ann Biomed Eng*. 2014;42:432–44. PMid:24468975. doi: https://doi.org/10.1007/s10439-014-0969-9.
48. Kumar A, Nune KC, Misra RDK. Biological functionality of extracellular matrix-ornamented three-dimensional printed hydroxyapatite scaffolds. *J Biomed Mater Res Part A*. 2016;104:1343–51. doi: https://doi.org/10.1002/jbm.a.35664.
49. Kuss MA, Wu S, Wang Y, Untrauer JB, Li W, Lim JY, Duan B. Prevascularization of 3D printed bone scaffolds by bioactive hydrogels and cell co-culture. *J Biomed Mater Res Part B Appl Biomater*. 2018;106:1788–98. doi: https://doi.org/10.1002/jbm.b.33994.
50. Lam CX., Mo X., Teoh S., Hutmacher D. Scaffold development using 3D printing with a starch-based polymer. *Mater Sci Eng C*. 2002;20:49–56. doi: https://doi.org/10.1016/S0928-

4931(02)00012-7.
51. Leukers B, Gülkan H, Irsen SH, Milz S, Tille C, Schieker M, Seitz H. Hydroxyapatite scaffolds for bone tissue engineering made by 3D printing. *J Mater Sci Mater Med*. 2005;16:1121–4. doi: https://doi.org/10.1007/s10856-005-4716-5.
52. Li H, He J, Yu H, Green CR, Chang J. Bioglass promotes wound healing by affecting gap junction connexin 43 mediated endothelial cell behavior. *Biomaterials*. 2016;84:64–75. doi: https://doi.org/10.1016/J.BIOMATERIALS.2016.01.033.
53. Li R, McCarthy A, Zhang YS, Xie J. Decorating 3D Printed Scaffolds with Electrospun Nanofiber Segments for Tissue Engineering. *Adv Biosyst*. 2019;3:1900137. doi: https://doi.org/10.1002/adbi.201900137.
54. Li VC, Kirschner MW. Molecular ties between the cell cycle and differentiation in embryonic stem cells. *Proc Natl Acad Sci U S A*. 2014;111:9503–8. PMid:24979803. doi: https://doi.org/10.1073/pnas.1408638111.
55. Lian JB, McKee MD, Todd AM, Gerstenfeld LC. Induction of bone-related proteins, osteocalcin and osteopontin, and their matrix ultrastructural localization with development of chondrocyte hypertrophy in vitro. *J Cell Biochem*. 1993;52:206–19. doi: https://doi.org/10.1002/jcb.240520212.
56. Liao J, Guo X, Grande-Allen KJ, Kasper FK, Mikos AG. Bioactive polymer/extracellular matrix scaffolds fabricated with a flow perfusion bioreactor for cartilage tissue engineering. *Biomaterials*. 2010a;31:8911–20. doi: https://doi.org/10.1016/j.biomaterials.2010.07.110.
57. Liao J, Guo X, Nelson D, Kasper FK, Mikos AG. Modulation of osteogenic properties of biodegradable polymer/extracellular matrix scaffolds generated with a flow perfusion bioreactor. *Acta Biomater*. 2010b;6:2386–93. doi: https://doi.org/10.1016/j.actbio.2010.01.011.
58. Lisignoli G, Toneguzzi S, Piacentini A, Cattini L, Lenti A, Tschon M, Cristino S, Grassi F, Facchini A. Human osteoblasts express functional CXC chemokine receptors 3 and 5: Activation by their ligands, CXCL10 and CXCL13, significantly induces alkaline phosphatase and β-N-acetylhexosaminidase release. *J Cell Physiol*. 2003;194:71–9. doi:

https://doi.org/10.1002/jcp.10188.
59. Liu S, Zhang H, Zhang X, Lu W, Huang X, Xie H, Zhou J, Wang W, Zhang Y, Liu Y, Deng Z, Jin Y. Synergistic angiogenesis promoting effects of extracellular matrix scaffolds and adipose-derived stem cells during wound repair. *Tissue Eng Part A*. 2011;17:725–39. PMid:20929282. doi: https://doi.org/10.1089/ten.TEA.2010.0331.
60. Liu YC, Kao YT, Huang WK, Lin KY, Wu SC, Hsu SC, Schuyler SC, Li LY, Lu FL, Lu J. CCL5/RANTES is important for inducing osteogenesis of human mesenchymal stem cells and is regulated by dexamethasone. *Biosci Trends*. 2014;8:138–43. doi: https://doi.org/10.5582/bst.2014.01047.
61. Lobel KD, Hench LL. In-vitro protein interactions with a bioactive gel-glass. *J Sol-Gel Sci Technol*. 1996;7:69–76. doi: https://doi.org/10.1007/BF00401885.
62. Lock A, Cornish J, Musson DS. The role of in vitro immune response assessment for biomaterials. *J Funct Biomater*. 2019;10. doi: https://doi.org/10.3390/jfb10030031.
63. Mascharak S, Benitez PL, Proctor AC, Madl CM, Hu KH, Dewi RE, Butte MJ, Heilshorn SC. YAP-dependent Mechanotransduction is Required for Proliferation and Migration on Native-like Substrate Topography HHS Public Access. *Biomaterials*. 2017;115:155–66. doi: https://doi.org/10.1016/j.biomaterials.2016.11.019.
64. McBeath R, Pirone DM, Nelson CM, Bhadriraju K, Chen CS. Cell Shape, Cytoskeletal Tension, and RhoA Regulate Stem Cell Lineage Commitment. *Dev Cell*. 2004;6:483–95. doi: https://doi.org/10.1016/S1534-5807(04)00075-9.
65. Miao Y, Chen Y, Liu X, DIao J, Zhao N, Shi X, Wang Y. Melatonin decorated 3D-printed beta-tricalcium phosphate scaffolds promoting bone regeneration in a rat calvarial defect model. *J Mater Chem B*. 2019;7:3250–9. doi: https://doi.org/10.1039/c8tb03361g.
66. Mihaila SM, Gaharwar AK, Reis RL, Khademhosseini A, Marques AP, Gomes ME. The osteogenic differentiation of SSEA-4 sub-population of human adipose derived stem cells using silicate nanoplatelets. *Biomaterials*. 2014;35:9087–99. PMid:25123923. doi:

https://doi.org/10.1016/j.biomaterials.2014.07.052.
67. Mitton-Fitzgerald E, Gohr CM, Bettendorf B, Rosenthal AK. The Role of ANK in Calcium Pyrophosphate Deposition Disease. *Curr Rheumatol Rep*. 2016;18:25. PMid:27032788. doi: https://doi.org/10.1007/s11926-016-0574-z.
68. Moore MC, Pandolfi V, Mcfetridge PS. Novel human-derived extracellular matrix induces in vitro and in vivo vascularization and inhibits fibrosis. 2015. doi: https://doi.org/10.1016/j.biomaterials.2015.01.022.
69. Mori G, Brunetti G, Oranger A, Carbone C, Ballini A, Muzio L Lo, Colucci S, Mori C, Grassi FR, Grano M. Dental pulp stem cells: osteogenic differentiation and gene expression. *Ann N Y Acad Sci*. 2011;1237:47–52. PMid:22082364. doi: https://doi.org/10.1111/j.1749-6632.2011.06234.x.
70. Motealleh A, Eqtesadi S, Civantos A, Pajares A, Miranda P. Robocast 45S5 bioglass scaffolds: in vitro behavior. *J Mater Sci*. 2017;52:9179–91. doi: https://doi.org/10.1007/s10853-017-0775-5.
71. Murphy CM, O'Brien FJ, Little DG, Schindeler A. Cell-scaffold interactions in the bone tissue engineering triad. *Eur Cell Mater*. 2013;26:120–32. PMid:24052425. .
72. Naruse K, Urabe K, Mukaida T, Ueno T, Migishima F, Oikawa A, Mikuni-Takagaki Y, Itoman M. Spontaneous differentiation of mesenchymal stem cells obtained from fetal rat circulation. *Bone*. 2004;35:850–8. PMid:15454092. doi: https://doi.org/10.1016/j.bone.2004.05.006.
73. Niu H, Lin D, Tang W, Ma Y, Duan B, Yuan Y, Liu C. Surface Topography Regulates Osteogenic Differentiation of MSCs via Crosstalk between FAK/MAPK and ILK/β-Catenin Pathways in a Hierarchically Porous Environment. *ACS Biomater Sci Eng*. 2017;3:3161–75. doi: https://doi.org/10.1021/acsbiomaterials.7b00315.
74. Noh YK, Du P, Kim IG, Ko J, Kim SW, Park K. Polymer mesh scaffold combined with cell-derived ECM for osteogenesis of human mesenchymal stem cells. *Biomater Res*. 2016;20. doi: https://doi.org/10.1186/s40824-016-0055-5.
75. Ohashi K, Fujiwara S, Mizuno K. Roles of the cytoskeleton, cell adhesion and rho signalling in mechanosensing and

mechanotransduction. *J Biochem*. 2017;161:mvw082. PMid:28082721. doi: https://doi.org/10.1093/jb/mvw082.
76. Orimo H. The mechanism of mineralization and the role of alkaline phosphatase in health and disease. *J Nippon Med Sch*. 2010;77:4–12. PMid:20154452. .
77. Pati F, Song TH, Rijal G, Jang J, Kim SW, Cho DW. Ornamenting 3D printed scaffolds with cell-laid extracellular matrix for bone tissue regeneration. *Biomaterials*. 2015;37:230–41. doi: https://doi.org/10.1016/j.biomaterials.2014.10.012.
78. Pierdomenico L, Bonsi L, Calvitti M, Rondelli D, Arpinati M, Chirumbolo G, Becchetti E, Marchionni C, Alviano F, Fossati V, Staffolani N, Franchina M, Grossi A, Bagnara GP. Multipotent mesenchymal stem cells with immunosuppressive activity can be easily isolated from dental pulp. *Transplantation*. 2005;80:836–42. PMid:16210973. .
79. Provenzano PP, Keely PJ. Mechanical signaling through the cytoskeleton regulates cell proliferation by coordinated focal adhesion and Rho GTPase signaling. *J Cell Sci*. 2011;124:1195–205. doi: https://doi.org/10.1242/jcs.067009.
80. Qi X, Wang H, Zhang Y, Pang L, Xiao W, Jia W, Zhao S, Wang D, Huang W, Wang Q. Mesoporous bioactive glass-coated 3D printed borosilicate bioactive glass scaffolds for improving repair of bone defects. *Int J Biol Sci*. 2018;14:471–84. doi: https://doi.org/10.7150/ijbs.23872.
81. Roberts SJ, Chen Y, Moesen M, Schrooten J, Luyten FP. Enhancement of osteogenic gene expression for the differentiation of human periosteal derived cells. *Stem Cell Res*. 2011;7:137–44. PMid:21763621. doi: https://doi.org/10.1016/j.scr.2011.04.003.
82. Rutkovskiy A, Stensløkken K-O, Vaage IJ. Osteoblast Differentiation at a Glance. *Med Sci Monit Basic Res*. 2016;22:95–106. PMid:27667570. doi: https://doi.org/10.12659/MSMBR.901142.
83. Salvay DM, Rives CB, Zhang X, Chen F, Kaufman DB, Lowe WL, Shea LD. Extracellular matrix protein-coated scaffolds promote the reversal of diabetes after extrahepatic islet transplantation. *Transplantation*. 2008;85:1456–64. doi: https://doi.org/10.1097/TP.0b013e31816fc0ea.

84. Saşmazel HT, Gümüşderelioğlu M, Gürpinar A, Onur MA. Comparison of cellular proliferation on dense and porous PCL scaffolds. *Biomed Mater Eng*. 2008;18:119–28. PMid:18725692. .
85. Scaffaro R, Lopresti F, Botta L, Rigogliuso S, Ghersi G. Integration of PCL and PLA in a monolithic porous scaffold for interface tissue engineering. *J Mech Behav Biomed Mater*. 2016;63:303–13. doi: https://doi.org/10.1016/J.JMBBM.2016.06.021.
86. Shanjani Y, Hu Y, Pilliar RM, Toyserkani E. Mechanical characteristics of solid-freeform-fabricated porous calcium polyphosphate structures with oriented stacked layers. *Acta Biomater*. 2011;7:1788–96. doi: https://doi.org/10.1016/J.ACTBIO.2010.12.017.
87. Silver IA, Deas J, Erecińska M. Interactions of bioactive glasses with osteoblasts in vitro: effects of 45S5 Bioglass, and 58S and 77S bioactive glasses on metabolism, intracellular ion concentrations and cell viability. *Biomaterials*. 2001;22:175–85. PMid:11101161. .
88. Soriente A, Fasolino I, Raucci MG, Demitri C, Madaghiele M, Giuri A, Sannino A, Ambrosio L. Effect of inorganic and organic bioactive signals decoration on the biological performance of chitosan scaffolds for bone tissue engineering. *J Mater Sci Mater Med*. 2018;29. doi: https://doi.org/10.1007/s10856-018-6072-2.
89. Srinivasan S, Jayasree R, Chennazhi KP, Nair SV, Jayakumar R. Biocompatible alginate/nano bioactive glass ceramic composite scaffolds for periodontal tissue regeneration. *Carbohydr Polym*. 2012;87:274–83. doi: https://doi.org/10.1016/J.CARBPOL.2011.07.058.
90. Su DL, Lu ZM, Shen MN, Li X, Sun LY. Roles of pro- and anti-inflammatory cytokines in the pathogenesis of SLE. *J Biomed Biotechnol*. 2012;2012. doi: https://doi.org/10.1155/2012/347141.
91. Su P, Tian Y, Yang C, Ma X, Wang X, Pei J, Qian A. Mesenchymal Stem Cell Migration during Bone Formation and Bone Diseases Therapy. *Int J Mol Sci*. 2018;19:2343. PMid:30096908. doi: https://doi.org/10.3390/ijms19082343.
92. Tamaki Y, Nakahara T, Ishikawa H, Sato S. In vitro analysis of

mesenchymal stem cells derived from human teeth and bone marrow. *Odontology*. 2013;101:121–32. PMid:22772774. doi: https://doi.org/10.1007/s10266-012-0075-0.
93. Tamburaci S, Tihminlioglu F. Biosilica incorporated 3D porous scaffolds for bone tissue engineering applications. *Mater Sci Eng C*. 2018;91:274–91. doi: https://doi.org/10.1016/J.MSEC.2018.05.040.
94. Tavakol S, Azami M, Khoshzaban A, Ragerdi Kashani I, Tavakol B, Hoveizi E, Rezayat Sorkhabadi SM. Effect of laminated hydroxyapatite/gelatin nanocomposite scaffold structure on osteogenesis using unrestricted somatic stem cells in rat. *Cell Biol Int*. 2013;37:n/a-n/a. PMid:23765607. doi: https://doi.org/10.1002/cbin.10143.
95. Thibault RA, Mikos AG, Kasper FK. Protein and mineral composition of osteogenic extracellular matrix constructs generated with a flow perfusion bioreactor. *Biomacromolecules*. 2011;12:4204–12. doi: https://doi.org/10.1021/bm200975a.
96. Urrutia CO, Dominguez-García MV, Flores-Estrada J, Laguna-Camacho A, Castillo-Cadena J, Flores-Merino M V. Mechanical Stimulation of Cells Through Scaffold Design for Tissue Engineering. Scaffolds Tissue Eng. - Mater. Technol. Clin. Appl., InTech; 2017. doi: https://doi.org/10.5772/intechopen.69925.
97. Valerio P, Pereira MM, Goes AM, Leite MF. The effect of ionic products from bioactive glass dissolution on osteoblast proliferation and collagen production. *Biomaterials*. 2004;25:2941–8. doi: https://doi.org/10.1016/J.BIOMATERIALS.2003.09.086.
98. Vila M, García A, Girotti A, Alonso M, Rodríguez-Cabello JC, González-Vázquez A, Planell JA, Engel E, Buján J, García-Honduvilla N, Vallet-Regí M. 3D silicon doped hydroxyapatite scaffolds decorated with Elastin-like Recombinamers for bone regenerative medicine. *Acta Biomater*. 2016;45:349–56. doi: https://doi.org/10.1016/j.actbio.2016.09.016.
99. Wall A, Board T. The Compressive Behavior of Bone as a Two-Phase Porous Structure. Class. Pap. Orthop., London: Springer London; 2014, p. 457–60. doi: https://doi.org/10.1007/978-1-4471-5451-8_116.

100. Xiao J, Dong H, Wu Y, Tian W, Liu L. Gene expression profiling of Cx3cl1 in bone marrow mesenchymal stem cells by osteogenic induction. *Omi A J Integr Biol*. 2009;13:337–43. doi: https://doi.org/10.1089/omi.2009.0018.
101. Xie Z, Tang S, Ye G, Wang P, Li J, Liu W, Li M, Wang S, Wu X, Cen S, Zheng G, Ma M, Wu Y, Shen H. Interleukin-6/interleukin-6 receptor complex promotes osteogenic differentiation of bone marrow-derived mesenchymal stem cells. *Stem Cell Res Ther*. 2018;9:13. doi: https://doi.org/10.1186/s13287-017-0766-0.
102. Xu J, Li Z, Hou Y, Fang W. Potential mechanisms underlying the Runx2 induced osteogenesis of bone marrow mesenchymal stem cells. *Am J Transl Res*. 2015;7:2527–35. PMid:26885254. .
103. Xynos ID, Edgar AJ, Buttery LD, Hench LL, Polak JM. Gene-expression profiling of human osteoblasts following treatment with the ionic products of Bioglass 45S5 dissolution. *J Biomed Mater Res*. 2001;55:151–7. PMid:11255166. .
104. Yang A, Lu Y, Xing J, Li Z, Yin X, Dou C, Dong S, Luo F, Xie Z, Hou T, Xu J. IL-8 Enhances Therapeutic Effects of BMSCs on Bone Regeneration via CXCR2-Mediated PI3k/Akt Signaling Pathway. *Cell Physiol Biochem*. 2018;48:361–70. doi: https://doi.org/10.1159/000491742.
105. Yao Q, Cosme JGL, Xu T, Miszuk JM, Picciani PHS, Fong H, Sun H. Three dimensional electrospun PCL/PLA blend nanofibrous scaffolds with significantly improved stem cells osteogenic differentiation and cranial bone formation. *Biomaterials*. 2017;115:115–27. doi: https://doi.org/10.1016/j.biomaterials.2016.11.018.
106. Yim EKF, Pang SW, Leong KW. Synthetic nanostructures inducing differentiation of human mesenchymal stem cells into neuronal lineage. *Exp Cell Res*. 2007;313:1820–9. PMid:17428465. doi: https://doi.org/10.1016/j.yexcr.2007.02.031.
107. Yu H, Peng J, Xu Y, Chang J, Li H. Bioglass Activated Skin Tissue Engineering Constructs for Wound Healing. *ACS Appl Mater Interfaces*. 2016;8:703–15. doi: https://doi.org/10.1021/acsami.5b09853.
108. Zhang H, Mao X, Du Z, Jiang W, Han X, Zhao D, Han D, Li Q.

Three dimensional printed macroporous polylactic acid/hydroxyapatite composite scaffolds for promoting bone formation in a critical-size rat calvarial defect model. *Sci Technol Adv Mater*. 2016;17:136. PMid:27877865. doi: https://doi.org/10.1080/14686996.2016.1145532.

109. Zhang S, Ma B, Liu F, Duan J, Wang S, Qiu J, Li D, Sang Y, Liu C, Liu D, Liu H. Polylactic Acid Nanopillar Array-Driven Osteogenic Differentiation of Human Adipose-Derived Stem Cells Determined by Pillar Diameter. *Nano Lett*. 2018;18:2243–53. doi: https://doi.org/10.1021/acs.nanolett.7b04747.
110. Zhu C, Rodda AE, Truong VX, Shi Y, Zhou K, Haynes JM, Wang B, Cook WD, Forsythe JS. Increased Cardiomyocyte Alignment and Intracellular Calcium Transients Using Micropatterned and Drug-Releasing Poly(Glycerol Sebacate) Elastomers. *ACS Biomater Sci Eng*. 2018:acsbiomaterials.8b00084. doi: https://doi.org/10.1021/acsbiomaterials.8b00084.
111. Zhu Y, Zhu R, Ma J, Weng Z, Wang Y, Shi X, Li Y, Yan X, Dong Z, Xu J, Tang C, Jin L. *In vitro* cell proliferation evaluation of porous nano-zirconia scaffolds with different porosity for bone tissue engineering. *Biomed Mater*. 2015;10:055009. doi: https://doi.org/10.1088/1748-6041/10/5/055009.
112. Rosen CJ, editor. Primer on the Metabolic Bone Diseases and Disorders of Mineral Metabolism. Ames, USA: John Wiley & Sons, Inc.; 2013. doi: https://doi.org/10.1002/9781118453926.

FINANCIAL SUPPORT

This work was supported by:

- The grant of Research Council of Lithuania, No. MIP – 046/2015;
- L'ORÉAL Baltic scholarship „For Women in Science";
- „INFOBALT" Association scholarship.

THE LIST OF PUBLICATIONS

1. Alksnė M, Šimoliūnas E, Kalvaitytė M, Skliutas E, Rinkūnaitė I, Gendvilienė I, Baltriukienė D, Rutkūnas V, Bukelskienė V. The effect of larger than cell diameter polylactic acid surface patterns on osteogenic differentiation of rat dental pulp stem cells. *J Biomed Mater Res A*. 2019;107(1):174-186. doi:10.1002/jbm.a.36547.

2. Alksnė M, Kalvaitytė M, Šimoliūnas E, Rinkūnaitė I, Gendvilienė I, Locs J, Rutkūnas V, Bukelskiene V. *In vitro* comparison of 3D printed polylactic acid/hydroxyapatite and polylactic acid/bioglass composite scaffolds: Insights into materials for bone regeneration. *J Mech Behav Biomed Mater*. 2020. doi: 10.1016/j.jmbbm.2020.103641.

THE LIST OF PRESENTATIONS

Oral presentations:

1. **Alksnė M,** Kalvaitytė M, Šimoliūnas E, Gendviliene I, Rutkūnas V, Bukelskiene V. Kaulinio audinio konstravimas panaudojant 3D karkasą ir nepilnos diferenciacijos ląsteles. „Thermo Fisher Scientific“ mokslo diena 2019; 2019 October 9; Vilnius, Lithuania.
2. **Alksnė M**, Kalvaitytė M, Šimoliūnas E, Bukelskienė V. Dirbtinio kaulinio audinio karkaso, sukonstruoto 3D spausdinimo būdu, savybių tyrimas *in vitro*. 9-oji jaunųjų mokslininkų konferencija „Fizinių ir technologijos mokslų tarpdalykiniai tyrimai“; 2019 March 12; The Lithuanian Academy of Sciences, Vilnius, Lithuania.
3. **Alksnė M**, Kalvaitytė M, Šimoliūnas E, Bukelskienė V. Dirbtinio kaulinio audinio karkaso, sukonstruoto 3D spausdinimo būdu, savybių tyrimas *in vitro*. INFOBALT stipendijų konkursas; 2019 March 18; INVL technologies, Vilnius, Lithuania.
4. **Alksnė M**, Kalvaitytė M, Šimoliūnas E, Bukelskienė V, Baltriukiene D. Macro-structured polylactic acid scaffolds for osteogenic differentiation. CellFit Workshop – Cells Communicate! 2019 March 14; Belgrade, Serbia.
5. **Alksnė M**. Micro-structured polylactic acid scaffolds for osteogenic regeneration. III International Conferencce of Lithuanian Association of Stem Cells Researchers; 2017 October 27; Vilnius, Lithuania.

Poster presentations:

1. Šimoliūnas E, **Alksnė M**, Kalvaitytė M, Bukelskienė V, Baltriukienė D. PLA composites and pure PLA decorated with cell-derived extracellular matrix impact on the fate of dental pulp stem cells osteogenic differentiation. CellFit Workshop – Cells Communicate! 2019 March 14; Belgrade, Serbia.

2. Kalvaitytė M, **Alksnė M**, Šimoliūnas E, Bukelkiene V. The Impact of Scaffold Microstructure on Dental Pulp Stem Cells Osteogenic Differentiation. The COINS`18. 2018 February 28-March 2; Vilnius, Lithuania.
3. Kalvaitytė M, **Alksnė M**, Šimoliūnas E, Bukelkiene V. The impact of PLA scaffold micro-structurization on rat's dental pulp stem cells osteogenic differentiation *in vitro*. The COINS`17. 2017 February 28-March 2; Vilnius, Lithuania.
4. **Alksnė M**, Šimoliūnas E, Kalvaitytė M, Skliutas E, Barasa P, Baltriukienė D, Bukelskienė V. The influence of ordered 3D printed PLA scaffold microstructurization on rat dental pulp stem cells. 2017 TERMIS-EU Conference; 2017 June 26-30; Davos, Switzerland.
5. **Alksnė M**, Gendvilienė I, Šimoliūnas E, Barasa P, Kalvaitytė M, Skliutas E, Malinauskas M, Baltriukienė D, Bukelskienė V, Rutkūnas V. The effect of ordered 3D printed PLA scaffold microstructurization on DPSC osteogenic differentiation in vitro and new bone formation *in vivo*. 20th Anniversary Conference Laboratory Animals in Research. 2016 November 24-25; Vilnius, Lithuania.
6. Barasa P, **Pečiukaitytė M**, Balčiūnas E, Šimoliūnas E, Baltriukienė D, Bukelskienė V. Influence of surface topography on the vital processes of myogenic cells in vitro. XIV International Conference of Lithuanian Biochemical Society. 2016 June 28-30; Druskininkai, Lithuania.

ACKNOWLEDGEMENTS

First of all, I would like to express sincere gratitude to my supervisor dr. Virginija Bukelskienė for opportunity to work and perform research in department of Biological Models, as well as for advice, comments, help, care and patience throughout this whole time.

For help, support, advice and ideas I thank my colleagues dr. Daiva Baltriukienė, prof. dr. Vygandas Rutkūnas, Miglė Kalvaitytė, Povilas Barasa, Egidijus Šimoliūnas, Ieva Rinkūnaitė and Ieva Gendvilienė.

I am grateful to my colleagues from Proteomics Center: dr. Mindaugas Valys, Silvija Urnikytė and Nadežda Dreižė for the HEK293T cell line, lentiviral vectors and advices on cell transfection.

My sincere thanks go to the Department of Cell Biology for the opportunity to use a fluorescent microscope.

I would also like to thank the Riga Institute of General Chemical Engineering for HA powder and the company 3D Creative for scaffold printing.

I thank all Institute of Biochemistry “cell-scientists” for keeping a good mood in the workplace.

Last but not least, I want to thank my whole family!

INFORMATION ABOUT THE AUTHOR

Milda Alksnė

Date of birth: August 3, 1989
Nationality: Lithuanian
E-mail: milda.peciukaityte@gf.vu.lt; milda.peciukaityte@gmail.com

Education

2014-2019 **Doctoral program in Natural Science, Biochemistry.**
Vilnius University (Institute of Biochemistry), Sauletekio av. 7, Vilnius (Lithuania).
PhD thesis "Substrate-dependent fate of stem cells: insights into artificial bone fabrication", supervisor dr. Virginija Bukelskienė.

2012-2014 **Master degree in Molecular biology.**
Vilnius University (Faculty of Natural Sciences), M.K. Čiurlionio 21/27, Vilnius (Lithuania).
Master thesis „ The Role of Stress-activated Protein kinases in Quinones-Induced MH-22A Cell Death“, supervisor dr. Virginija Bukelskienė.

2012-2013 **FELASA C category certificate.**
Vilnius University (Faculty of Natural Sciences), M.K.Čiurlionio 21/27, Vilnius (Lithuania).
Certificate for work with laboratory animals.

2008-2012 **Bachelor degree in biology, molecular biology speciality**.
Vilnius University (Faculty of Natural Sciences), M.K.Čiurlionio 21/27, Vilnius (Lithuania)
Bachelor thesis “ Comparison of Aziridinylbenzoquinones, RH1 and MeDZQ, Effect In Mouse Hepatoma Cells", supervisor dr. Virginija Bukelskienė

Awards

2019 L'ORÉAL Baltic 'For Women in Science' scholarship.
2019 The INFOBALT scholarship for young scientists.
2016 „BAFF Professional Internship Program" scholarship.

Memberships

2015 Lithuanian Association of Stem Cell Researchers.
2012 Lithuanian Biochemical Society.
2010 Baltic Laboratory Animal Science Association.

Scientific interests

- Stem cell behaviour and their use in tissue regeneration .
- Construction of artificial tissues/ organs *in vitro* and their *in vivo* testing .
- Cytotoxicity studies *in vitro* and *in vivo*.

Academic experience

Milda Alksnė is a co-author of eight scientific publications in the field of biochemistry and has presented 30 oral and poster presentations in local and international conferences and symposiums.

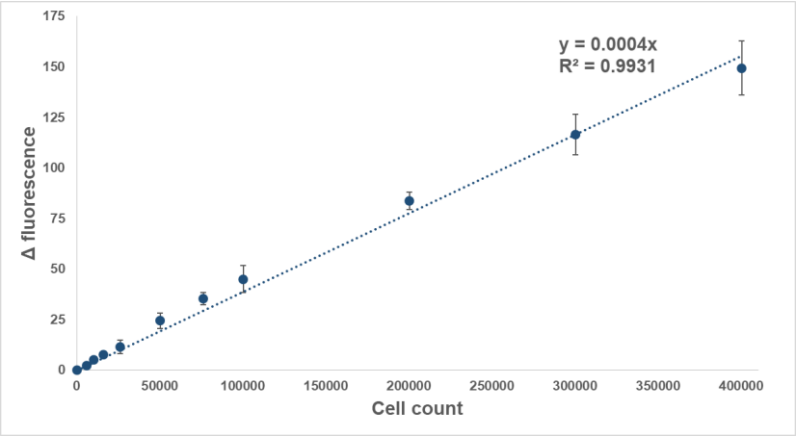

S1 Figure. DAPI correlation to cell number calibration curve. Calibration curves (n = 3) mean values are plotted in the graph. Error bars represent ± SD.

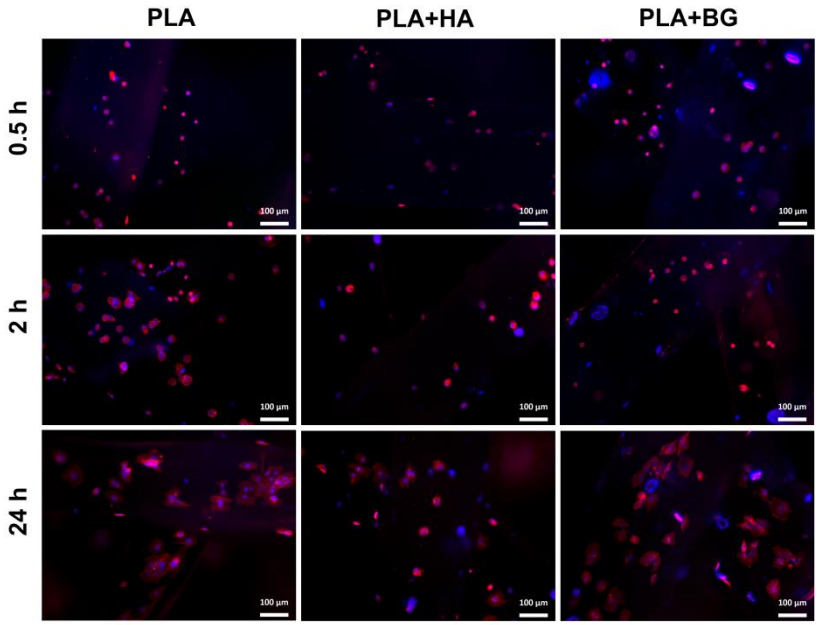

S2 Figure. DPSC morphology changes on different surfaces after cultivation for 0.5, 2 and 24 h on tested scaffolds.
Immunofluorescently stained cell nuclei (DAPI, blue) and F-actin filaments (rhodamine phalloidin, red).

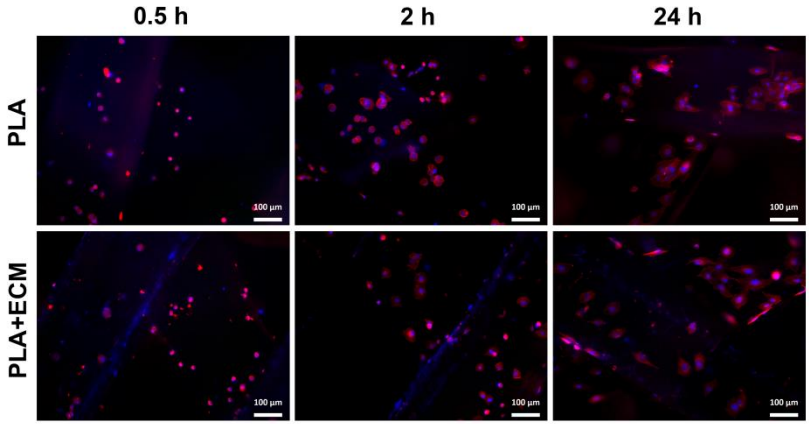

S3 Figure. DPSC morphology changes on different surfaces after cultivation for 0.5, 2 and 24 h on ECM coated and pure PLA scaffolds. Immunofluorescently stained cell nuclei (DAPI, blue) and F-actin filaments (rhodamine phalloidin, red).

A

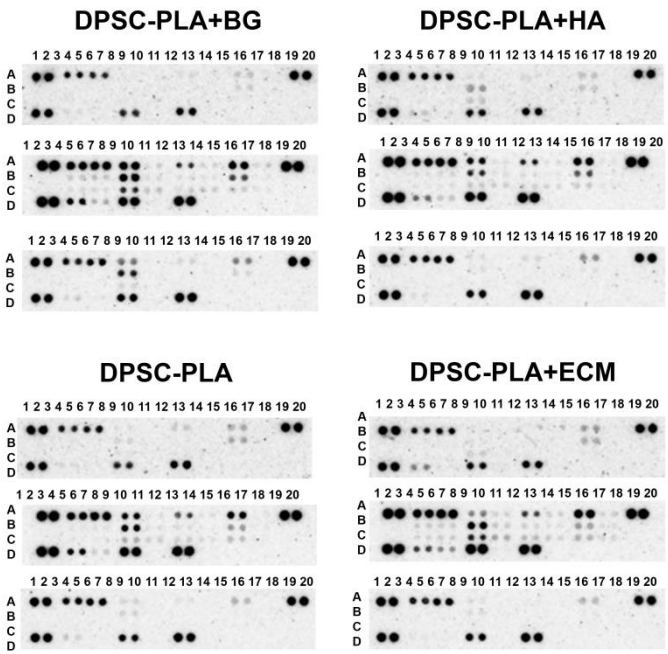

B

Cytokines, chemokines and growth factor layout																			
	1	2	3	4	5	6	7	8	9	10	11	12	13	14	15	16	17	18	19	20
A	Reference Spots		CINC-1		CINC-2α/β		CINC-3		CNTF		CX3CL1		GM-CSF		sICAM-1		IFN- γ		Reference Spots	
B			IL-1α		IL-1β		IL-1ra		IL-2		IL-3		IL-4		IL-6		IL-10			
C			IL-13		IL-17		CXCL10		LIX		L-Selectin		MIG		MIP-1α		MIP-3α			
D	Reference Spots		CCL5		CXCL7		TIMP-1		TNF-α		VEGF						Negative Control			

Figure S4. Analysis of cytokines, chemokines and growth factors present in constructs' secretomes. A – qualitative images of tested molecules, obtained by Dot Blot assay; B – coordinates of investigated molecules and controls.

Vilnius University Publishing House
9 Saulėtekio Av., Building III, LT-10222 Vilnius
Email: info@leidykla.vu.lt, www.leidykla.vu.lt
Print run 15 copies